South African Journal of Botany 185 (2025) 66–79

Contents lists available at ScienceDirect

South African Journal of Botany

journal homepage: www.elsevier.com/locate/sajb

Chemical constituents of the leaves and roots of *Lantana camara* Linn (Verbenaceae) display good *in vitro* antiplasmodial potency and ADMET properties

Pierre Leonel K.Tafokeu Taguimjeu [a,b], Mariscal Brice Tchatat Tali [c,d], Kevine Johane Jumeta Dongmo [b], Yannick Stéphane Fotsing Fongang [e,*], Marie-Laure Fauconnier [a,*], Bruno Ndjakou Lenta [f], Fabrice Fekam Boyom [c,d], Norbert Sewald [g], Silvère Augustin Ngouela [b]

[a] *Laboratory of Chemistry of Natural Molecules, Gembloux Agro-Bio Tech, University of Liège, Passage des Déportés 2, 5030 Gembloux, Belgium*
[b] *Department of Organic Chemistry, Faculty of Science, University of Yaoundé I, P.O. Box 812, Yaoundé, Cameroon*
[c] *Antimicrobial and Biocontrol Agents Unit, Faculty of Science, University of Yaoundé I, P.O. Box 812 Yaoundé, Cameroon*
[d] *Advanced Research & Health Innovation Hub, P.O. Box 20133, Yaoundé, Cameroon*
[e] *Department of Chemistry, Higher Teachers' Training College, The University of Maroua, P.O. Box 55 Maroua, Cameroon*
[f] *Department of Chemistry, Higher Teachers Training College, University of Yaoundé I, P.O. Box 49, Yaoundé, Cameroon*
[g] *Organic and Bioorganic Chemistry, Department of Chemistry, Bielefeld University, P.O. Box 100131, 33501 Bielefeld, Germany*

ARTICLE INFO

Edited by Editor: Dr S.C. Pendota

Keywords:
Malaria
Lantana camara
Antiplasmodial assay
Haemolysis assay
Furanonaphthoquinones
Natural products (NPs)
ADMET prediction

ABSTRACT

The emergence of artemisinin-resistant parasites in Africa highlights the need to expand the arsenal of new antimalarial lead pharmacophores with good pharmacological properties and novel mechanisms of action, particularly those derived from natural products. *Lantana camara* L. is a medicinal plant historically used to treat various ailments, including malaria. Decoctions of its leaves and roots have traditionally been used in endemic regions to treat the disease. However, a thorough validation of its efficacy through the identification of its antimalarial chemical pharmacophores has never been achieved. The purpose of this study was to unveil antiplasmodial chemical "hits" from the leaves and roots of L. *camara* coupled with *in silico* predictions of their pharmacokinetic properties and drug-likeness. Crude ethanolic and EtOAc-MeOH (12:13; *v/v*) extracts were obtained through the maceration of L. *camara* leaves and roots. Subsequently, fractionation was performed, and all fractions were assessed for their activity against chloroquine-susceptible (*Pf*3D7) and multidrug-resistant (*Pf*Dd2) strains of *Plasmodium falciparum* using the SyBr Green fluorescence-based methods. The antiplasmodial "hit" compounds were isolated through flash silica chromatography followed by successive column chromatography. The obtained compounds were then subjected to *in vitro* evaluation against the same strains (*Pf*3D7 and *Pf*Dd2). Virtual *in silico* prediction using an open Artificial Intelligence and Machine Learning (AI/ML)-assisted tool named pKSCM predictor was used to retrieve the pharmacokinetic (ADMET) properties of the potent antiplasmodial scaffolds. The ethanolic leaf and EtOAc-MeOH root extracts of L. *camara* showed moderate antiplasmodial activity against both chloroquine-sensitive (*Pf*3D7) and multidrug-resistant (*Pf*Dd2) *P. falciparum* strains. Notably, the RF2 root fraction exhibited significant activity, particularly against *Pf*Dd2 (IC_{50} = 7.73 μg/mL). From this fraction, a binary mixture of furanonaphthoquinones [diodantunezone (**1a**) and isodiodantunezone (**1b**) (2:1)] was isolated, showing strong potency against both parasite strains (IC_{50} = 2.59 μg/mL [12.10 μM] for *Pf*Dd2 and 6.05 μg/mL [28.27 μM] for *Pf*3D7). The compounds were non-toxic to erythrocytes and selective for intraerythrocytic parasites. *In silico* prediction of ADMET (absorption, distribution, metabolism, and toxicity parameters further supported their drug-like properties. This study provides the first evidence of the antiplasmodial efficacy of L. *camara* extracts and derivatives, with an emphasis on their drug-like ability, supporting its traditional use against malaria.

* Corresponding authors.
E-mail addresses: pltaguimjeu@uliege.be, taguimjeuleonel@outlook.fr (P.L.K.Tafokeu Taguimjeu), b.tchatat@yahoo.com (M.B. Tchatat Tali), jumetakevine@yahoo.fr (K.J.J. Dongmo), fongangfys@yahoo.fr (Y.S.F. Fongang), marie-laure.fauconnier@uliege.be (M.-L. Fauconnier), lentabruno@yahoo.fr (B.N. Lenta), fabrice.boyom@fulbrightmail.org (F.F. Boyom), norbert.sewald@uni-bielefeld.de (N. Sewald), sngouela@yahoo.fr (S.A. Ngouela).

https://doi.org/10.1016/j.sajb.2025.07.039
Received 30 April 2025; Received in revised form 26 June 2025; Accepted 25 July 2025

Abbreviations

ACTs	Artemisinin-Based Combination Therapies
ADMET	Absorption, Distribution, Metabolism, Excretion, and Toxicity
Art	Artemisinin
BBB	Limited Blood-brain Barrier
CC_{50}	Median Cytotoxic Concentrations
CC	Column Chromatography
CNS	Central Nervous System
CQ	Chloroquine
DMEM	Dulbecco's modified Eagle's medium
FEBLC	Leaves crude extract of L. *camara*
FFALC	Ethyl acetate fraction of L. *camara*
FFHLC	*n*-Hexane fraction of L. *camara*
Ffnbu	*n*-butanol fraction
Fr.	Fraction
HNC	Cameroon National Herbarium
Hz	Hertz
IC_{50}	Median inhibitory concentration
IC_{50} *Pf*Dd2	Median Inhibitory Concentration against *Plasmodium falciparum* Dd2 strain
IC_{50} *Pf*3D7	Median Inhibitory Concentration against *Plasmodium falciparum* 3D7 strain
ITMs	Improved Traditional Medicines
J	Coupling constant (in Hertz)
MS	Mass Spectrometry
NMR	Nuclear Magnetic Resonance
NPs	Natural products
Pf	*Plasmodium falciparum*
REBLC	Roots crude extract L. *camara*
RF	Root fraction
RF_M	Root fraction mixture
RI	Resistance Index
SD	Standard Deviation
SI	Selectivity Index
TLC	Thin Layer Chromatography
WHO	World Health Organization

1. Introduction

New and recurring infectious diseases represent a continuous threat to global health security (Dongmo et al., 2023; Nkengasong and Tessema, 2020; WHO, 2020). The current global situation with COVID-19 clearly demonstrates this assertion. Notwithstanding the rise of COVID-19, malaria continues to be a significant global public health issue, with sub-Saharan African countries accounting for most cases and deaths related to this disease. Among *Plasmodium* species, *Plasmodium falciparum* remains the most virulent and major cause of severe malaria in patients (WHO, 2023; 2021a; 2021b; Sato, 2021; Taguimjeu et al., 2025). Many cases and fatalities are predominant in sub-Saharan Africa. Nonetheless, substantial numbers of cases and deaths are also reported in the WHO regions Southeast Asia, the Eastern Mediterranean, the Western Pacific, and the Americas. In 2023, approximately 263 million malaria cases led to nearly 597 000 deaths globally, with 95 % of these cases occurring in Africa, and 76 % of deaths being children under the age of 5 (WHO, 2024). Current malaria treatments in Africa target potentially drug-resistant malaria parasites using artemisinin-based combination therapies (ACTs). A significant challenge to malaria control continues to be the emergence of resistance to ACTs, particularly in the Greater Mekong Sub-region and, more recently, in Africa (Asua et al., 2021; Rosenthal, 2021). Therefore, if artemisinin-resistant strains of *P. falciparum* develop in or are brought to Africa, it would have dire consequences for malaria control across the continent (Tali et al., 2022). Considering these health challenges, an imperative need to identify new active, safe, and more effective antimalarial drugs with innovative mechanisms of action to tackle resistant pathogens and roll back the burden of malaria has become increasingly critical (Dongmo et al., 2023; Ariey et al., 2014).

Historically, medicinal plants have supplied medicine in the fight against malaria as it was the case for quinine isolated from *Cinchona* spp. and artemisinin isolated from *Artemisia* spp. Natural products offer a vast potential for discovering new drugs due to their unparalleled chemical diversity (Fongang et al., 2021; Aman, 2019). Hence, investigating plants currently used in folk medicine for malaria treatment could provide future drugs (Atanasov et al., 2015; Venkatesalu et al., 2012).

Lantana camara Linn (Verbenaceae) [syn. *Camara vulgaris* Benth., *Lantana bahamensis* f. albiflora Moldenke, L. *coccinea Lodd*. Ex G. Don, L. *glandulossima* f. aculeatissima Moldenke, L. *mexicana* Turner, and L. *spinosa* L. ex Le Cointe, according to the database https://wfoplantlist.org] is an attractive ornamental shrub native to Mexico, the Caribbean, and Tropical South Africa, but that have spread throughout many tropical and subtropical locations of the world (Cullen and Stalker, 2016). It is well recognized as a natural mosquito repellent and has found various applications in traditional medicine across many regions of the world to treat chickenpox, swelling, cancer, tumours, eczema, asthma, ulcers, bilious fevers, rheumatism, catarrhal infections, hypertension, and malaria (Tabuti, 2008; Njoroge and Bussmann, 2006). This plant is known in Cameroon by local populations as *kangwé* (in Douala), *ngong* (in Ewondo), *tchindap* ou Nglang (in Bassa), and *elok nkunda* (in Beti) (Ntiga, 2008). Its fresh leaves and bark decoctions are taken orally to treat toothache and fever, respectively (Kambele et al., 2022; Shipa et al., 2022; Nea et al., 2021; Tamdem et al., 2020; Mayori, 2017). In the East and Littoral regions of Cameroon, the decoction of the fresh leaves of L. *camara* is taken orally to treat malaria, while in the Adamaoua region, the whole plant *Bidens pilosa* added to fresh leaves of L. *camara* is boiled and drunk for the same purpose (Tsague, 2019; Dibong et al., 2011). In Dschang in the West Region of Cameroon, where the plant was harvested, it is called *Lekekueh* (*Yembâ*) by local people. Its leaves are boiled with leaves of *Carica papaya* and the whole plant of *Cymbopogon citratus* to treat malaria. In South Africa, where L. *camara* is known as an invasive plant called "*Tshidzimbampotolo*" in *Tshivenda*, its leaves are used to treat colds and eye pain, while an infused mixture of leaves and roots is drunk to treat kwashiorkor (Cock and Van Vuuren, 2020; Mahwasane et al., 2013). Previous research on this plant has primarily focused on characterizing its phytochemical profiles and, in some instances, randomly testing extracts or compounds for biological activities (antibacterial, antimycobacterial, antifungal, etc.). Chemical investigations showed that it contains terpenoids, alkaloids, flavonoids, saponins, carbohydrates, saponins, steroids, and tannins (Boakye et al., 2023; Qureshi et al., 2019; Baba et al., 2011; Herbert et al., 1991). However, no studies have employed a systematic approach to assess the bioactivities of this plant by selecting extracts or fractions based on their antiplasmodial potency for further investigation.

In this context, we carried out a bio-guided investigation of L. *camara* antiplasmodial activities coupled with its absorption, distribution, metabolism, excretion, and toxicity (ADMET) properties to search for molecules that can be used for the development of new therapeutic agents against malaria with suitable application. Hence, this study reports the antiplasmodial potency of extracts, fractions, and some compounds obtained from L. *camara* coupled with *in silico* prediction of pharmacokinetics and drug-likeness related properties.

2. Materials and methods

2.1. Plant sample collection and processing

The leaves and roots of *Lantana camara* [known in Cameroon by local populations as *kangwé* (in Douala), *ngong* (in Ewondo), *tchindap* or Nglang (in Bassa), and *elok nkunda* (in Beti), *Lekekueh* (*Yembâ*), in English as common lantana, big-sage, white-sage, and tickberry] were harvested in Foto-Dschang (5°26′38.3"N 10°3′12"E), Menoua Subdivision, West region of Cameroon, in September 2020. The taxonomic

identification of the plant was confirmed by Mr. Victor Nana, a skilled botanist at the Cameroon National Herbarium (HNC), and compared with an existing specimen registered under voucher number 34855HNC. The plant's scientific name was checked on the website https://wfoplantlist.org on October 28, 2024, and https://www.theplantlist.org on December 3rd, 2024.

2.2. Isolation and characterization of secondary metabolites

The roots were chopped, dried in the shade, and crushed, yielding 4.2 kg of powder. The powder was extracted with an EtOAc-MeOH (12:13; *v/v*) mixture by maceration at room temperature for 72 h. The filtrates were freed from solvent under vacuum to yield 280.1 g of crude extract. Similarly, freshly collected leaves of L. *camara* were air-dried for two weeks at room temperature, crushed into powder (2.5 kg) and extracted twice by maceration with ethanol (15 L) for three days (24 *h* × 3) and evaporated to dryness under pressure at low temperature yielding 226.1 g of a dark-green extract.

Part of the roots crude extract (278.6 g) was subjected to vacuum liquid chromatography over silica gel eluting with *n*-hexane, *n*-hexane/EtOAc, EtOAc/MeOH and MeOH to afford six fractions labelled RF_1 (16.4 g), RF_2 (10.8 g), RF_3 (39.1 g), RF_4 (43.9 g), RF_5 (33.7 g), and RF_6 (47.1 g), respectively. Fraction RF_1 was a complex mixture of fats that was not investigated. Fraction RF_2 (10.0 g) was subjected to CC over silica gel and eluted with *n*- hexane/acetone (9:1 – 1:1) to provide a mixture of diodantunezone and isodiodantunezone (**1a** + **1b**, 15.2 mg). Fractions RF_3 (38.0 g) and RF_4 (42.0 g) were pooled together based on the results of the antiplasmodial assay and their TLC profile into one pool named RF_M (83.6 g). Part of the RF_M fraction (82.0 g) was purified over a silica gel CC and eluted with *n*- hexane/EtOAc (1:0 – 0:1) and EtOAc/MeOH (1:0 – 4:1) mixtures to provide a mixture of stigmasterol and *β*-sitosterol (**14a** + **14b**, 24.1 mg), lantadene A (**3**, 36.3 mg), oleanonic acid (**5**, 69.1 mg), and oleanolic acid (**6**, 981.8 mg). Fraction RF_5 (32.0 g) was separated by CC over silica gel eluting, with *n*- hexane/EtOAc (19:1 – 0:1) and with EtOAc/MeOH (1:0 – 9:1) mixtures to afford lantanolic acid (**2**, 25.4 mg). RF_6 was a complex mixture of polar compound that was not investigated.

Part of the leaf crude extract (225.0 g) was suspended in distilled water (1 L) and successively exhausted with *n*-hexane (2 L), EtOAc (2 L), and *n*-BuOH (1 L) to give 74.1 g, 51.34 g, and 69.22 g of each solvent fraction, respectively. Part of the *n*-hexane fraction (73.0 g) was subjected to CC silica over gel with the *n*- hexane/EtOAc (1:0 – 0:1) and EtOAc/MeOH (1:0 – 4:1) mixtures as eluent to afford four subfractions (Fr. 1 to Fr. 4). Purification of the subfraction Fr. 1 (19.04 g) *n*-hexane/acetone (19:1 – 9:1) yielded betulinic acid (**8**, 13.2 mg) and a mixture of sterol (stigmasterol and *β*-sitosterol) (**14a** + **14b**, 16.2 mg), while the purification of the subfraction Fr. 2 (29.03 g) with *n*- hexane/acetone (9:1 – 1:3) afforded a mixture of 5-hydroxy-7,4′-dimethoxyflavone and eupatorin (**10a** + **10b**, 5.1 mg) and ursolic acid (**7**, 6.7 mg). The subfraction Fr. 3 (18.7 g) was eluted with *n*- CH_2Cl_2/EtOAc (19:1) to yield 13^2-*epi*-phaeophorbide-A ethyl ester (**12**, 10.1 mg) and lantadene A (**3**, 7.1 mg), while the subfraction Fr. 4 (15.4 g) was subjected to CC over silica gel eluting with *n*-hexane/EtOAc (7:11 – 0:1) mixtures to afford 3-*O*-*β*-d-glucopyranoside *β*-sitosterol (**15**, 25.1 mg). Part of the EtOAc fraction (50.0 g) was eluted with *n*-hexane/EtOAc/MeOH (1:1 – 1:0 then 1:0 – 4:1) to afford lantadene A (**3**, 84.2 mg), lantadene B (**4**, 7.2 mg), oleanonic acid (**5**, 45.1 mg), oleanolic acid (**6**, 10.4 mg), lupeol (**9**, 5.2 mg), apigenin (**11**, 6.1 mg), and a complex mixture Fr. (10.2 g). This mixture Fr. 7 (10.2 g) was subsequently chromatographed on silica gel, with *n*-hexane/EtOAc (4:1) was subjected to CC over Sephadex LH-20 with MeOH as eluent to yield cholesteryl pentadecanoate (**13**, 9.1 mg). The remaining fractions and subfractions were not studied due to their complexity.

2.3. General procedures and structure elucidation

NMR spectra were measured on a Bruker Avance AV-500 spectrometer at 600 and 150 MHz for ^1H and ^{13}C, respectively, with solvent peaks as references. The chemical shifts (δ) were reported in ppm, while coupling constants (*J*) were reported in hertz (Hz). A series of column chromatography separations was carried out with silica gel (230 – 400 mesh), and vacuum liquid chromatography was conducted with silica gel (70 – 230 mesh). Fractions were monitored by thin layer chromatography (TLC); TLC was conducted on precoated silica gel 60 F_{254} plates (Merck), and the TLC spots were visualized with a UV lamp at 254 and 365 nm, and by spraying the plates with 50 % aqueous sulphuric acid and heating at 80 °C for few minutes.

2.4. UPLC-Q-TOF-MS/MS and ESI-MS/MS method for chemical profile and analysis

ESI-MS/MS analysis was performed using a triple quadrupole mass spectrometer (QqQ) coupled to an electrospray ionization (ESI) source (Ghallab et al., 2021). The positive ionization mode was used, as it demonstrated greater selectivity and sensitivity for the analysis of targeted metabolites. The electrospray ionization (ESI) source operated under the following conditions: the capillary and cone voltages were set at 3.5 kV and 1 kV, respectively. The ion source temperature was maintained at 150 °C, while the pressure of the nitrogen gas (nebulizer) was adjusted to 35 psi. The drying and sheath gas (N_2) were heated to 350 °C, and their flow rates were set at 13 and 8 L/min, respectively. To acquire MS spectra, a mass-to-charge ratio (*m/z*) range of 20–300 m/z was applied. For MS/MS fragmentation analyses, a collision gas (nitrogen) with an energy ramp ranging from 5 to 50 eV was employed. MS^n experiments were conducted under the same MS conditions as described above.

2.5. Biological assay

2.5.1. In vitro inhibition of P. falciparum asexual-blood stages

2.5.1.1. Parasite culture and maintenance. Fresh *O*+ human red blood cells were utilized to culture the chloroquine-sensitive [*Pf*3D7-(MRA-102)] and multidrug-resistant [*Pf*Dd2-(MRA-150)] strains of *Plasmodium falciparum* at a haematocrit concentration of 4 % in complete RPMI 1640 medium. This solution was prepared by incorporating 500 mL RPMI 1640 (Gibco, UK), with 25 mM HEPES (Gibco, UK), 0.5 % Albumax I (Gibco, USA), 1X hypoxanthine (Gibco, USA) and 50 mg/mL gentamicin (Gibco, China). The culture was maintained at a temperature of 37 °C in an optimal environment with 5 % CO_2. The medium was changed daily to propagate the culture. Thin blood smears stained with Giemsa were examined under a microscope with immersion oil to monitor the transition of the cell cycle and the progression of parasitaemia. Ring stage parasites were acquired by serial treatment with 5 % D-sorbitol two days before every experiment (Lambros and Vanderberg, 1979).

2.5.1.2. SYBR Green fluorescence-based assay. Drug sensitivity tests were performed in 96-well microtiter plates using a SYBR Green I fluorescence-based technique (Smilkstein et al., 2004). This approach depends on the ability of SYBR Green to produce intense fluorescence when parasite DNA is present due to cellular proliferation. The lack of a nucleus in human red blood cells, where the malarial parasite multiplies, allows the specific use of SYBR Green to track the proliferation of the malarial parasite. Experimentally, sorbitol-synchronized ring-stage parasites (haematocrit: 1 %, parasitaemia: 2 %, 90 μL) were incubated under standard culture conditions for 72 h at 37 °C with prediluted extracts, fractions, isolated compounds, and a reference drug (10 μL).

After incubation, 100 μL of SYBR Green I buffer, which consist of 6 μL

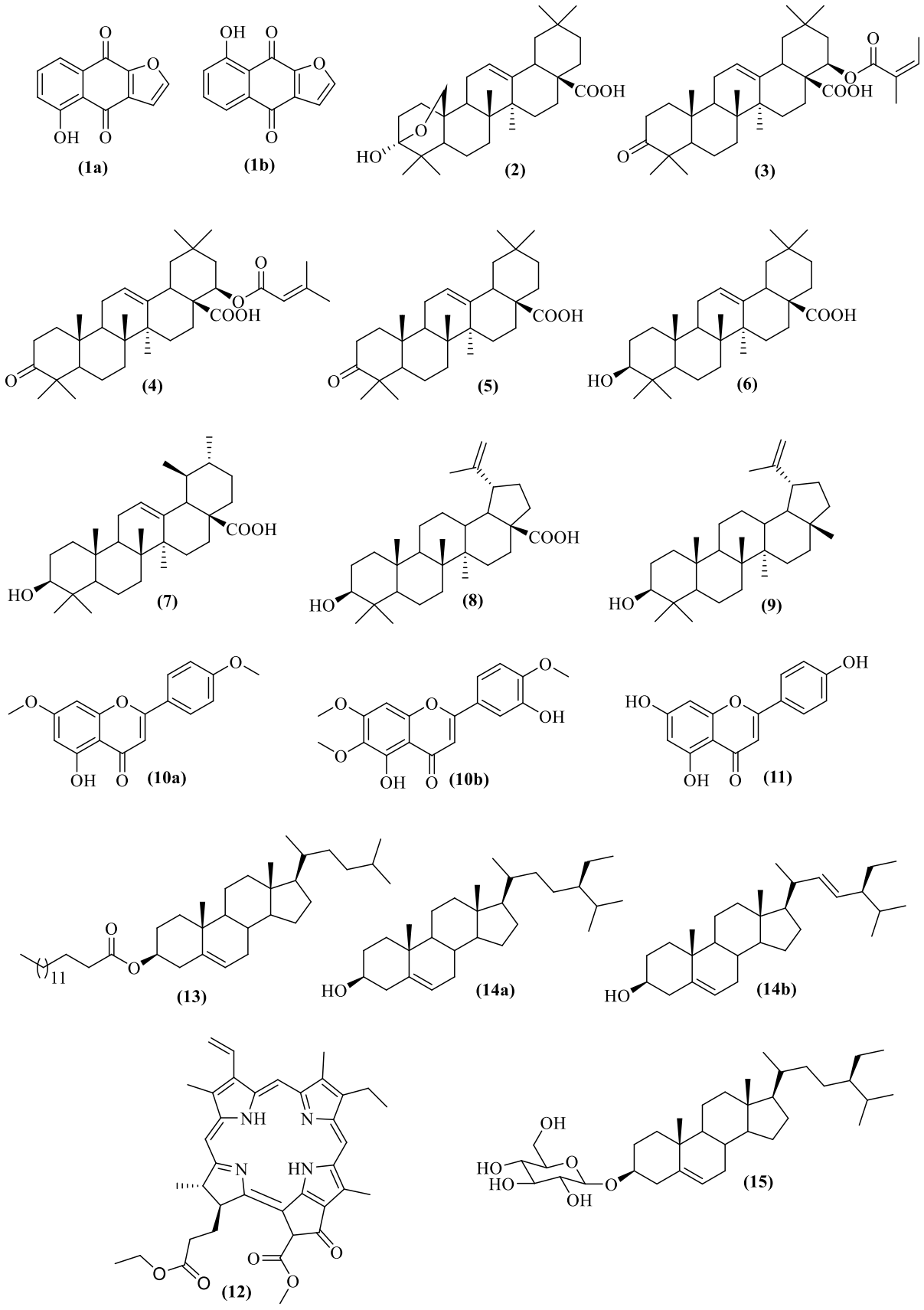

Fig. 1. Structures of compounds isolated from L. *camara.*

of 10,000 × SYBR Green I (Invitrogen), 600 μL of red blood cell lysis buffer (Tris at 25 mM, pH 7.5), 360 μL of EDTA (7.5 mM), 19.2 μL of parasite lysis solution (saponin at 0.012 %; w/v), and 28.8 μL of Triton X-100 (0.08 %; *v/v*), was introduced to each well, and incubated in the dark for one hour at 37 °C. Thereafter, fluorescence was measured using an Infinite M200 Microplate reader (TECAN) with excitation and emission wavelengths configured at 485 and 538 nm, respectively. The fluorescence counts were utilized to calculate the percentage of inhibition using Microsoft Excel. The 50 % inhibitory concentration (IC_{50}) was determined by analysing dose-response curves using GraphPad Prism 8.0. Experiments were performed in triplicate and repeated three times with similar results.

$$\%\,\text{Haemolysis} = \frac{\text{Absorbance of sample 415 nm} - \text{Absorbance of blank sample 415 nm}}{\text{Absorbance of positive control 415 nm}} \times 100$$

2.5.2. Resistance index (RI)

The level of resistance was assessed by comparing the activity of each inhibitor on the chloroquine-sensitive (*Pf*3D7) and multidrug-resistant (*Pf*Dd2) strains of *P. falciparum* using the provided formula: RI = IC_{50}*Pf*Dd2/IC_{50}*Pf*3D7 (Smit et al., 2015).

2.5.2.1. In vitro resazurin-based cytotoxicity assay. The isolated compounds cytotoxicity was evaluated using a resazurin-based assay (Bowling et al., 2012) on VERO cells grown in complete Dulbecco's Modified Eagle's Medium (DMEM). This medium was composed of 13.5 g/L DMEM (Sigma Aldrich), 10 % Foetal Bovine Serum (Sigma Aldrich), 0.2 % sodium bicarbonate (*w/v*) (Sigma Aldrich), and 50 μg/mL gentamicin (Sigma Aldrich). Macrophages were plated in 96-well flat-bottom cell culture plates at a density of 10,000 cells in 100 μL of complete medium per well and incubated for 24 h at 37 °C in a 5 % CO_2 atmosphere to promote cell adhesion. After the adhesion period, the medium was swapped out for new culture medium, consisting of 90 μL of complete medium and 10 μL of each test sample solution, which was serially diluted.

Control wells included a growth control (0.1 % DMSO representing 100 % growth) and a positive control using podophyllotoxin at 20 μM. To evaluate cell proliferation, 10 μL of a resazurin stock solution (0.15 mg/mL in sterile phosphate-buffer saline) was introduced to each well, after which a subsequent incubation of 4 h was carried out under identical culture conditions. Fluorescence readings were obtained using an Infinite M200 microplate reader (Tecan) at excitation/emission wavelengths of 530/590 nm. The results were expressed as 50 % cytotoxic concentrations (CC_{50}), and selectivity indices (CC_{50} VERO cell/IC_{50} *Pf*3D7/*Pf*Dd2) were determined for each tested compound.

2.5.2.2. Haemolysis assay. The haemolytic effect was examined by incubating normal erythrocytes with all the previously mentioned compounds in phosphate-buffered saline (PBS), as outlined by Sinha et al. (2019) with minor adjustments. In summary, fresh erythrocytes were centrifuged for 5 min at 1600 rpm for at least three times, and then the leftover pellet was resuspended in PBS at 4 % haematocrit. A total of one hundred microliters of the suspended pellet was introduced into a 96-well sterile culture plate containing test compounds at a final concentration of 200 μg/mL. PBS alone (for baseline values) and 0.4 % Triton X-100 in PBS (for 100 % haemolysis) served as controls. After a 3 h incubation at 37 °C, the test samples were centrifuged, and the supernatant was used to determine the haemolytic activity, which was quantified by measuring the haemoglobin release spectrophotometrically at an absorbance of 415 nm. Experiments were conducted three times, each sample in triplicate, and the mean ± SD was calculated (Kaushik et al., 2012).

3. Computational prediction of pharmacokinetic properties and drug-likeness of promising compounds

The most active (IC_{50} < 10 μg/mL) antiplasmodial compounds were submitted to computational pharmacokinetics prediction using the pkCSM predictor as described by Pires and collaborators (2015) to evaluate their potential to be developed as a future antimalarial drug candidate. To achieve this, the Simplified Molecular Input Line Entry Specification (SMILES) of the selected compounds and positive controls (Artemisinin and chloroquine) were extracted from the chemical structure and utilized as input to the pkCSM predictor, which forecasts small-molecule pharmacokinetic properties using graph-based signatures (http://biosig.unimelb.edu.au/pkcsm/). The tool is dynamic and curated with experimental data to simultaneously foresee multiple properties associated with pharmacokinetics (absorption, distribution, metabolism, excretion, and toxicity).

4. Results and discussion

4.1. Isolation and structure elucidation

To validate these solvent choices, micro-extractions were carried out using different solvent systems (methanol, dichloromethane-methanol (1:1), ethanol-water (7:3), ethanol and ethyl acetate-methanol (12:13), followed by comparative thin layer chromatography (TLC). These analyses identified the solvents with the most enriched secondary metabolite profiles. Based on these results, ethanol and ethyl acetate: methanol (12:13, *v/v*) were selected as the extraction solvents for leaves and roots, respectively. The leaf and the root extracts were subjected to silica gel and Sephadex LH-20 column chromatography (CC) to afford eighteen compounds (**1** – **15**). The chemical structures of these isolated and characterized compounds are shown in Fig. 1.

The structures of the compounds were identified as follows: a mixture of two co-isolated isomers, diodantunezone (**1a**) and isodiodantunezone (**1b**) (Dominguez et al., 1983); lantanolic acid (**2**) (Barre et al., 1997); lantadene A (**3**) (Suryati et al., 2019); lantadene B (**4**) (Delgado-Altamirano et al., 2021); oleanonic acid (**5**) (Wen et al., 2008); oleanolic acid (**6**), ursolic acid (**7**), betulinic acid (**8**), and lupeol (**9**) (Mahato and Kundu, 1994); a mixture of two co-isolated functional isomers, 5-hydroxy-7,4′-dimethoxyflavone (**10a**) (Mangoyi et al., 2015) and eupatorin (**10b**) (Ramaraj et al., 2018); apigenin (**11**) (Fajriah et al., 2016); 132-*epi*-phaeophorbide-A ethyl ester (**12**) (Camron et al., 1972; Sousa et al., 2018); cholesteryl pentadecanoate (**13**); a mixture of *β*-sitosterol (**14a**) and stigmasterol (**14b**); and 3-O-*β*-d-glucopyranoside of *β*-sitosterol (**15**) (Mahato and Kundu, 1994). These identifications were made by comparing their spectroscopic data with those previously reported in the literature.

***Diodantunezone* (1a) *and isodiodantunezone* (1b):** Orange powder; δ ^{1}H NMR ($CDCl_3$, 600 MHz): 7.02 (2H, *dd, J* = 7.5 Hz, 1.8 Hz), 7.29 (1H, *d, J* = 5.2 Hz), 7.64 (1H, *td, J* = 8.0; 5.2 Hz), 7.80 (2H, *d, J* = 2.0 Hz), 7.78 (1H, *d, J* = 1.7 Hz) 7.79 (1H, *d, J* = 3.3 Hz), 8.22 (1H, *m*), 8.25 (1H, *m*), 12.04 (1H, *s*, OH), 12.21 (1H, *s*, OH). ^{13}C NMR ($CDCl_3$, 150 MHz): 173.6 (C-1a), 172.8 (C-1b), 180.5 (C-4a and C-4b), 162.4 (C-8a and C-5b) (Dominguez et al., 1983).

***Lantanolic acid* (2):** White powder; δ ^{1}H NMR ($CDCl_3$, 600 MHz):

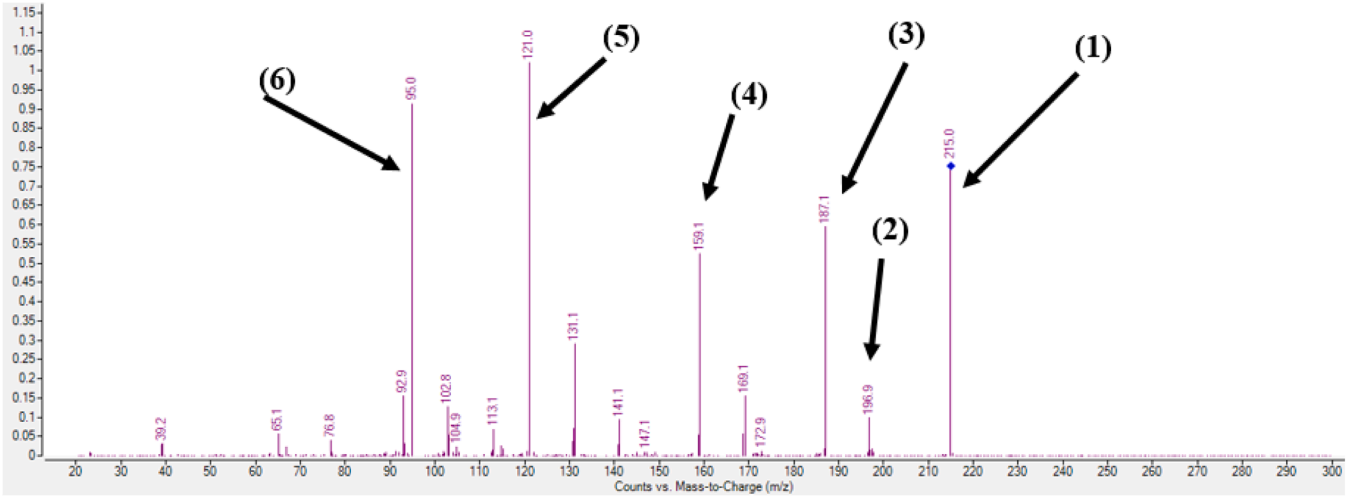

Fig. 2. UPLC-ESI-MS/MS chromatogram of diodantunezone and isodiodantunezone (**1a** + **1b**).

5.33 (1H, *t, J* = 3.8 Hz, H-12), 2.85 (1H, *dd, J* = 13.8; 3.7 Hz, H-18), 4.23 (1H, *dd, J* = 8.38; 2.27 Hz, H-25a), 3.91 (1H, *dd, J* = 8.38; 2.27 Hz, H-25b). ^{13}C NMR ($CDCl_3$, 150 MHz): 33.9 (C-1), 27.7 (C-2), 98.4 (C-3), 40.3 (C-4), 50.2 (C-5), 19.8 (C-6), 31.1 (C-7), 38.3 (C-8), 50.2 (C-9), 35.1 (C-10), 23.1 (C-11), 122.3 (C-12), 143.4 (C-13), 41.7 (C-14), 28.3 (C-15), 23.7 (C-16), 46.6 (C-17), 41.6 (C-18), 45.7 (C-19), 30.7 (C-20), 34.6 (C-21), 32.2 (C-22), 27.1 (C-23), 17.6 (C-24), 67.7 (C-25), 18.2 (C-26), 25.3 (C-27), 181.9 (C-28), 33.0 (C-29), 23.5 (C-30) (Barre et al., 1997).

Lantadene A (**3**): white powder; δ ^{1}H NMR ($CDCl_3$, 500 MHz): 1.50 (1H, *m*, H-1) / 1.92 (1H, *m*, H-1), 2.38 (1H, *m*, H-2) / 2.56 (1H, *m*, H-2), 1.31 (1H, *m*, H-5), 5.38 (1H, *t, J* = 3.7 Hz, H-12), 3.07 (1H, *dd, J* = 14.0; 4.5 Hz, H-18), 5.09 (1H, *t, J* = 3.2 Hz, H-22), 0.90 (3H, *s*, H-29), 1.00 (3H, *s*, H-30), 6.02 (1H, *dd, J* = 7.3; 1.6 Hz, H-33), 1.77 (3H, *d, J* = 1.7 Hz, H-34), 1.98 (3H, *d, J* = 1.6 Hz, H-35). ^{13}C NMR ($CDCl_3$, 125 MHz): 39.2 (C-1), 34.2 (C-2), 217.7 (C-3), 47.5 (C-4), 55.4 (C-5), 19.6 (C-6), 32.3 (C-7), 39.3 (C-8), 47.0 (C-9), 36.9 (C-10), 23.6 (C-11), 122.6 (C-12), 143.1 (C-13), 42.1 (C-14), 27.7 (C-15), 24.2 (C-16), 50.7 (C-17), 38.6 (C-18), 46.0 (C-19), 30.1 (C-20), 37.8 (C-21), 75.9 (C-22), 26.5 (C-23), 21.6 (C-24), 15.2 (C-25), 16.9 (C-26), 25.8 (C-27), 179.1 (C-28), 33.8 (C-29), 26.2 (C-30), 166.4 (C-31), 127.7 (C-32), 139.2 (C-33), 20.7 (C-34), 15.8 (C-35) (Suryati et al., 2019).

Lantadene B (**4**): white powder; δ ^{1}H NMR ($CDCl_3$, 500 MHz): 1.49 (1H, *m*, H-1a) / 1.92 (1H, *m*, H-1b), 2.38 (1H, *m*, H-2) / 2.56 (1H, *m*, H-2), 1.66 (1H, *m*, H-5), 5.39 (1H, *t, J* = 3.7 Hz, H-12), 3.04 (1H, *dd, J* = 13.7; 4.5 Hz, H-18), 5.05 (1H, *t, J* = 3.2 Hz, H-22), 0.85 (3H, *s*, H-29), 1.01 (3H, *s*, H-30), 5.57 (1H, *s*, H-32), 2.14 (3H, *s*, H-34), 1.85 (3H, *s*, H-35). ^{13}C NMR ($CDCl_3$, 125 MHz): 38.6 (C-1), 34.1 (C-2), 217.7 (C-3), 47.5 (C-4), 55.4 (C-5), 19.6 (C-6), 32.3 (C-7), 39.3 (C-8), 47.0 (C-9), 36.9 (C-10), 23.6 (C-11), 122.4 (C-12), 143.0 (C-13), 42.1 (C-14), 27.7 (C-15), 24.2 (C-16), 50.7 (C-17), 38.6 (C-18), 46.0 (C-19), 30.1 (C-20), 37.8 (C-21), 75.9 (C-22), 26.5 (C-23), 21.6 (C-24), 15.2 (C-25), 16.9 (C-26), 25.8 (C-27), 179.1 (C-28), 33.8 (C-29), 26.2 (C-30), 165.3 (C-31), 116.0 (C-32), 157.2 (C-33), 20.2 (C-34), 27.4 (C-35) (Delgado-Altamirano et al., 2021).

Oleanonic acid (**5**): White powder; δ ^{1}H NMR ($CDCl_3$, 600 MHz): White powder; δ ^{1}H NMR ($CDCl_3$, 600 MHz): 2.55 (1H, *m*, H-2a) / 2.38 (1H, *m*, H-2b)), 5.32 (1H, *t*, H-12), 2.86 (1H, *dd*, H-18). ^{13}C NMR ($CDCl_3$, 150 MHz): 39.1 (C-1), 34.2 (C-2), 217.7 (C-3), 47.4 (C-4), 55.3 (C-5), 19.5 (C-6), 32.4 (C-7), 39.6 (C-8), 46.9 (C-9), 36.6 (C-10), 22.8 (C-11), 122.3 (C-12), 143.5 (C-13), 41.7 (C-14), 27.4 (C-15), 23.8 (C-16), 46.7 (C-17), 41.1 (C-18), 45.6 (C-19), 31.0 (C-20), 33.8 (C-21), 32.2 (C-22), 26.8 (C-23), 21.4 (C-24), 15.0 (C-25), 17.5 (C-26), 25.8 (C-27), 183.9 (C-28), 33.4 (C-29), 23.6 (C-30) (Wen et al., 2008; Mahato and Kundu, 1994).

Oleanolic acid **(6):** White powder; δ ^{1}H NMR ($CDCl_3$, 600 MHz): 3.51 (1H, *dd*, H-3), 5.36 (1H, *t*, H-12), 3.31 (1H, *dd*, H-18). ^{13}C NMR ($CDCl_3$, 150 MHz): 39.0 (C-1), 28.1 (C-2), 78.2 (C-3), 39.4 (C-4), 55.9 (C-5), 18.8 (C-6), 33.4 (C-7), 39.8 (C-8), 48.2 (C-9), 37.4 (C-10), 23.8 (C-11), 122.6 (C-12), 144.8 (C-13), 42.2 (C-14), 28.4 (C-15), 23.8 (C-16), 46.7 (C-17), 42.1 (C-18), 46.6 (C-19), 31.0 (C-20), 34.3 (C-21), 33.2 (C-22), 28.8 (C-23), 16.5 (C-24), 15.6 (C-25), 17.5 (C-26), 26.2 (C-27), 180.0 (C-28), 33.4 (C-29), 23.8 (C-30) (Mahato and Kundu, 1994).

Ursolic acid **(7):** White powder; δ ^{1}H NMR ($CDCl_3$−MeOH (1:1), 600 MHz): 3.15 (1H, *q*, H-3), 5.34 (1H, *t*, H-12), 2.20 (1H, *d*, H-18). ^{13}C NMR ($CDCl_3$−MeOH (1:1), 150 MHz): 39.8 (C-1), 27.8 (C-2), 79.7 (C-3), 39.9 (C-4), 56.6 (C-5), 17.8 (C-6), 34.3 (C-7), 40.2 (C-8), 40.7 (C-9), 37.9 (C-10), 21.7 (C-11), 126.7 (C-12), 139.5 (C-13), 40.3 (C-14), 29.2 (C-15), 25.3 (C-16), 43.2 (C-17), 54.2 (C-18), 38.0 (C-19), 35.9 (C-20), 31.7 (C-21), 36.8 (C-22), 28.8 (C-23), 16.4 (C-24), 16.1 (C-25), 17.7 (C-26), 24.3 (C-27), 181.6 (C-28), 19.4 (C-29), 24.3 (C-30) (Mahato and Kundu, 1994).

Betulinic acid (**8**): White crystals; δ ^{1}H NMR ($CDCl_3$, 600 MHz): 3.21 (1H, *dd*, 10.0; 5.0 Hz, H-3), 3.02 (1H, *dd, J* = 9.6 ; 5.4 Hz, H-19), 4.56 (1H, *d, J* = 2.6 Hz, H-29), 4.69 (1H, *d, J* = 2.6 Hz, H-29′), 1.65 (3H, *s*, H-30). ^{13}C NMR ($CDCl_3$, 150 MHz): 36.2 (C-1), 27.1 (C-2), 76.7 (C-3), 38.4 (C-4), 54.8 (C-5), 17.9 (C-6), 33.9 (C-7), 40.4 (C-8), 49.9 (C-9), 37.6 (C-10), 20.4 (C-11), 25.0 (C-12), 38.2 (C-13), 41.9 (C-14), 30.1 (C-15), 31.6 (C-16), 55.3 (C-17), 46.5 (C-18), 48.6 (C-19), 150.2 (C-20), 29.1 (C-21), 36.7 (C-22), 27.9 (C-23), 15.8 (C-24), 15.6 (C-25), 15.7 (C-26), 14.3 (C-27), 177.0 (C-28), 109.4 (C-29), 18.9 (C-30) (Mahato and Kundu, 1994).

Lupeol (**9**): White powder; δ ^{1}H NMR ($CDCl_3$, 600 MHz): 3.22 (1H, *dd, J* = 6.1; 2.0 Hz, H-3), 4.59 (1H, *s*, H-29a), 4.71 (1H, *s*, H-29b). ^{13}C NMR ($CDCl_3$, 150 MHz): 38.1 (C-1), 27.4 (C-2), 79.0 (C-3), 38.7 (C-4), 55.3 (C-5), 18.3 (C-6), 34.3 (C-7), 40.8 (C-8), 50.4 (C-9), 37.2 (C-10), 20.9 (C-11), 25.1 (C-12), 38.9 (C-13), 42.8 (C-14), 27.4 (C-15), 35.6 (C-16), 43.0 (C-17), 48.3 (C-18), 48.0 (C-19), 151.0 (C-20), 29.8 (C-21), 40.0 (C-22), 28.0 (C-23), 15.4 (C-24), 16.1 (C-25), 16.0 (C-26), 14.5 (C-27), 18.0 (C-28), 109.3 (C-29), 19.3 (C-30) (Mahato and Kundu, 1994).

5-hydroxy-7,4′-dimethoxyflavone (**10a**) and ***eupatorin*** (**10b**): Yellow powder; δ ^{1}H NMR (Acetone-d_6, 600 MHz): 13.14 (1H, *s*, OH-5b), 9.13 (1H, *s*, OH-3′b) / 12.68 (1H, *s*, OH-5a), / 6.62 (1H, *s*, H-3a and 3b), 6.30 (1H, *d, J* = 2.2 Hz, H-6a), 6.61 (1H, *d, J* = 2.2 Hz, H-8a), 6.62 (1H, *s*, H-8b), 3.87 (3H, *s*, 7-OMe-a) / 3.88 (3H, *s*, 4′-OMe-a), 3.90 (3H, *s*, 6-OMe-b) / 3.91 (3H, *s*, 7-OMe-b) / 3.95 (3H, *s*, 4′-OMe-b). ^{13}C NMR (Acetone-d_6, 150 MHz): 103.2 (C-3a and 3b), 178.7 (C-4a) / 182.6 (C-4b), 97.6 (C-6a), 91.9 (C-8a) /, 111.0 (C-3′a and C-5′a), 114.5 (C-6′b) (Mangoyi et al., 2015; Ramaraj et al., 2018).

Apigenin (**11**): yellow powder; δ ^{1}H NMR (Methanol-d_4, 500 MHz): 6.61 (1H, *s*, H-3), 6.22 (1H, *d, J* = 2.1 Hz, H-6), 6.47 (1H, *d, J* = 2.1 Hz, H-8), 7.87 (2H, *d, J* = 8.4 Hz, H-2′/H-6′), 6.95 (2H, *d, J* = 8.4 Hz, H-3′/H-

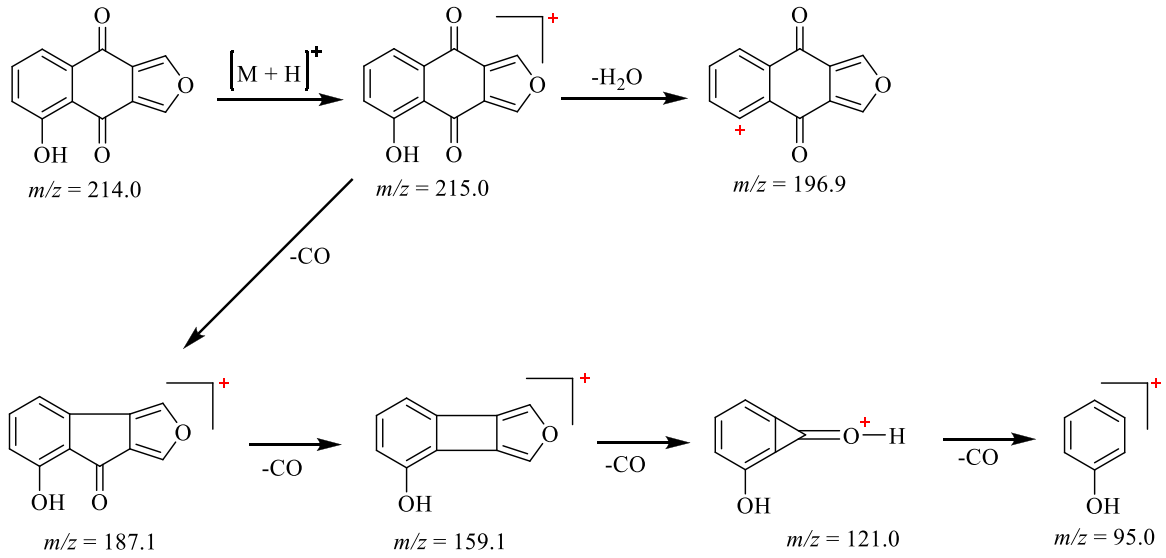

Scheme 1. MS/MS fragmentation pathway of diodantunezone and isodiodantunezone (**1a** + **1b**).

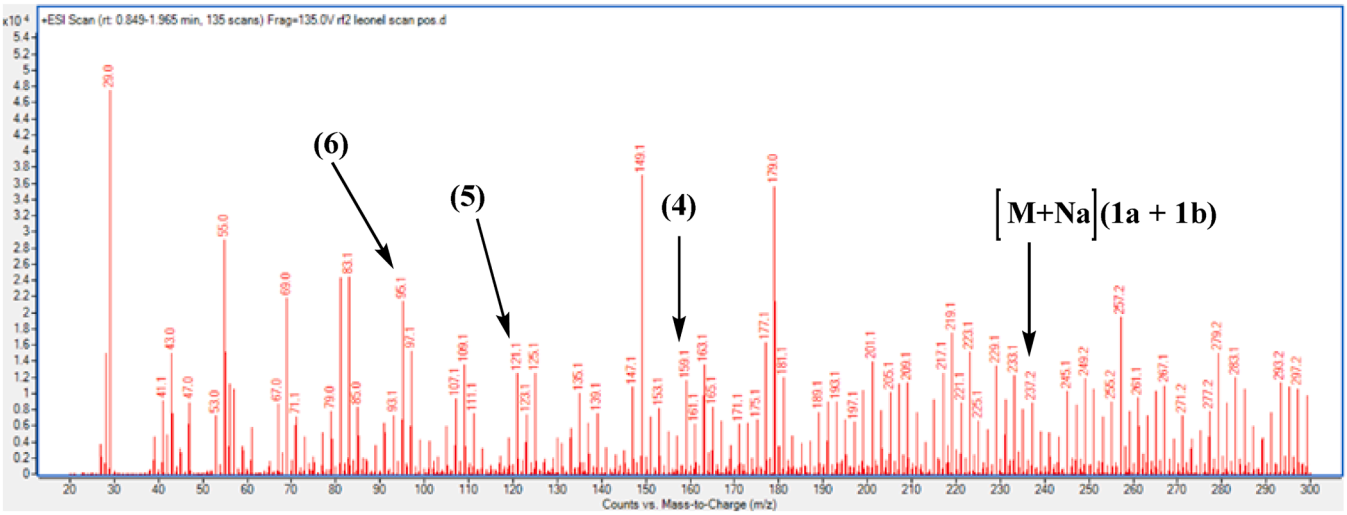

Fig. 3. UPLC-ESI-MS/MS chromatogram of the fraction RF_2 from the roots of L. *camara*.

5′). ^{13}C NMR (Methanol-d_4, 125 MHz): 164.9 (C-2), 102.4 (C-3), 182.5 (C-4), 161.8 (C-5), 98.9 (C-6), 164.8 (C-7), 93.7 (C-8), 158.06 (C-9), 103.8 (C-10), 121.8 (C-1′), 128.0 (C-2′/C-6′), 115.6 (C-3′/C-5′), 161.4 (C-4′) (Fajriah et al., 2016).

13^2-epi-phaeophorbide-A ethyl ester (**12**): green powder; δ ^{1}H NMR (Acetone-d_6, 500 MHz): 3.44 (3H, *s*, H-2^1), 8.10 (1H, *dd, J* = 17.8; 11.6 Hz, H-3^1), 6.34 (1H, *dd, J* = 11.6; 1.4 Hz, H-3^{2a}) / 6.20 (1H, *dd, J* = 11.6; 1.4 Hz, H-3^{2b}), 9.39 (1H, *s*, H-5), 3.15 (3H, *s*, H-7^1), 3.64 (2H, *m*, H-8^1), 1.64 (3H, *t, J* = 7.5 Hz, H-8^2), 9.68 (1H, *s*, H-10), 3.65 (3H, *s*, H-12^1), 6.25 (1H, *s*, H-13^2), 3.89 (3H, *s*, H-13^4), 3.94 (2H, *q, J* = 7.1 Hz, H-17^4), 1.01 (3H, *t, J* = 7.1 Hz, H-17^5), 4.66 (1H, *q, J* = 7.5 ; 2.2 Hz, H-18), 1.85 (3H, *d, J* = 7.3 Hz, H-18^1), 8.90 (1H, *s*, H-20). ^{13}C NMR (Acetone-d_6, 125 MHz): 142.1 (C-1), 131.9 (C-2), 12.1 (C-2^1), 136.1 (C-3), 129.0 (C-3^1), 122.7 (C-3^2), 136.2 (C-4), 97,5 (C-5), 155,7 (C-6), 136.2 (C-7), 11.2 (C-7^1), 145.2 (C-8), 19.4 (C-8^1), 17.4 (C-8^2), 151.0 (C-9), 104.4 (C-10), 137.8 (C-11), 129.0 (C-12), 12.1 (C-12^1), 128.3 (C-13), 189.3 (C-13^1), 64.8 (C-13^2), 169,8 (C-13^3), 52.9 (C-13^4), 149.7 (C-14), 105.0 (C-15), 161,5 (C-16), 51.2 (C-17), 30.0 (C-17^1), 31.1 (C-17^2), 173.3 (C-17^3), 59.8 (C-17^4), 13.4 (C-17^5), 50.2 (C-18), 23.1 (C-18^1), 172.3 (C-19), 93.2 (C-20) (Camron et al., 1972; Sousa et al., 2018).

Diodantunezone and isodiodantunezone (**1a** + **1b**) were isolated as an inseparable mixture of isomers from *Lanthana achyranthifolia* (Dominguez et al., 1983). Their structures are supported herein by their NMR data (Figures S2 – S7) and furthermore by the mass spectrometry through the interpretation of the molecular weight and the characteristic fragment ions obtained by MS/MS (Fig. 2). The positive ion mode was selected due to its better sensitivity and separation, and six major peaks were observed. The protonated ion $[M + H]^+$peak was detected at *m/z* 215.0 (Fig. 2). Its MS/MS spectrum revealed a series of characteristic fragments at *m/z* 215.0 (**1**), 196.9 (**2**), 187.1 (**3**), 159.1 (**4**), 121.1 (**5**), and 95.0 uma (**6**), attributable to 1,4-furanoanthraquinones bearing phenolic groups (Stensen and Jensen, 1995; Ye et al., 2007; Zhan et al., 2016), confirming the structures of diodantunezone and isodiodantunezone (**1a** + **1b**) (Scheme 1).

The mixture of isodiodantunezone and diodantunezone (**1a** + **1b**) was identified in fraction RF_2 of the root extract of L. *camara* (Fig. 3). Indeed, the interpretation of ESI-MS/MS data obtained from the positive electrospray mode of the fraction RF_2 allowed the identification of the major fragments from the mixture (**1a** + **1b**), especially the sodium adduct peak $[M + Na]^+$ at *m/z* 237.2, and those at *m/z* 187.1, 159.1 (**4**), 121.1 (**5**), and 95.0 (**6**), hence confirming the presence of diodantunezone and isodiodantunezone (**1a** + **1b**) in this fraction.

Table 1
Antiplasmodial activity and resistance index of leaf and root extracts of L. *camara* against *Plasmodium falciparum* strains.

Plants parts	Crude extracts code	Antiplasmodial activity IC_{50} ± SD (μg/mL)		Resistance Index: IC_{50}*Pf*Dd2/IC_{50}*Pf*3D7
		***Pf*3D7**	***Pf*Dd2**	
Leaves	FEBLC	14.31 ± 1.68	35.95 ± 2.21	2.51
Roots	REBLC	11.36 ± 0.59	18.07 ± 3.11	1.59
Positive Control	Artemisinin (μM)	0.03 ± 0.00	0.05 ± 0.01	1.66
	Chloroquine (μM)	0.02 ± 0.00	0.56 ± 0.10	28

4.2. Antiplasmodial results

Crude extracts, fractions, and compounds from L. *camara* were tested *in vitro* for their antiplasmodial potency against both chloroquine-sensitive (*Pf*3D7) and multidrug-resistant (*Pf*Dd2) strains of *P. falciparum*. The results obtained were classified based on the classification criteria [$IC_{50} \leq 5$ μg/mL: pronounced activity; $5 < IC_{50} \leq 10$ μg/mL: good activity; $10 < IC_{50} \leq 20$ μg/mL: moderate activity; $20 < IC_{50} \leq 40$ μg/mL: low activity; $IC_{50} > 40$ μg/mL: inactive.] previously described (Muganza et al., 2016). The findings indicated that, the root extract (REBLC) exhibited strong activity against both *Pf*3D7 and *Pf*Dd2, while the leaf extract (FEBLC) exhibited moderate activity against *Pf*3D7 and low activity against *Pf*Dd2 (Table 1). In a previous study, the dichloromethane-methanol extract of L. *camara* leaves from South Africa also demonstrated moderate activity against the *Pf*D10 strain, with an IC_{50} of 11 μg/mL (Tajbakhsh et al., 2021).

Importantly, fractions obtained from both extracts displayed good to moderate antiplasmodial activity against both strains of *P. falciparum*, with IC_{50} values ranging from 7.73 to > 30.63 μg/mL (Figs. 4 and 5; Table 2). Out of the nine fractions assessed, six exhibited moderate antiplasmodial activity against *Pf*3D7, while four demonstrated moderate activity against *Pf*Dd2. Interestingly, fraction R_2LC from roots displayed good activity against *Pf*Dd2, while fraction FFALC from the leaves displayed good activity against *Pf*3D7 and was therefore subjected to CC. Overall, 09 isolated compounds were assessed against both strains and exhibited varying degrees of activity with IC_{50} values ranging from 8.51 to 140.82 μM on *Pf*3D7 and from 12.10 to 71.40 μM on *Pf*Dd2 (Table 3). Among the tested compounds, oleanonic acid (**5**) displayed moderate activity against *Pf*3D7 with an IC_{50} value of 24 μM, and good activity against *Pf*Dd2 with an IC_{50} value of 20.79 μM. Interestingly, the mixture of diodantunezone (**1a**) and isodiodantunezone (**1b**) was the most active on both strains, with good (IC_{50} 28.27 μM [6.05

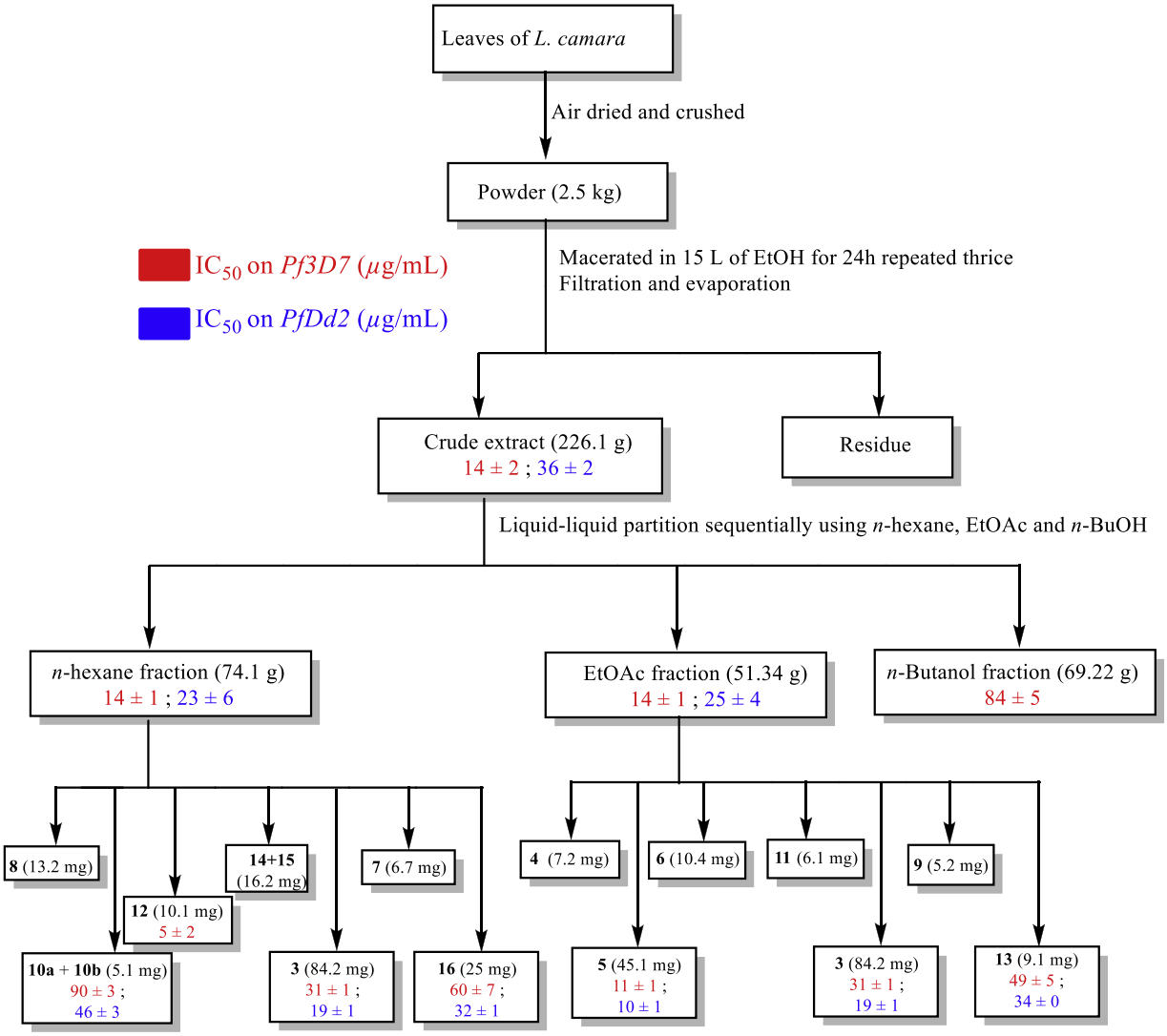

Fig. 4. Protocol of extraction and isolation of compounds from leaves of L. *camara*.

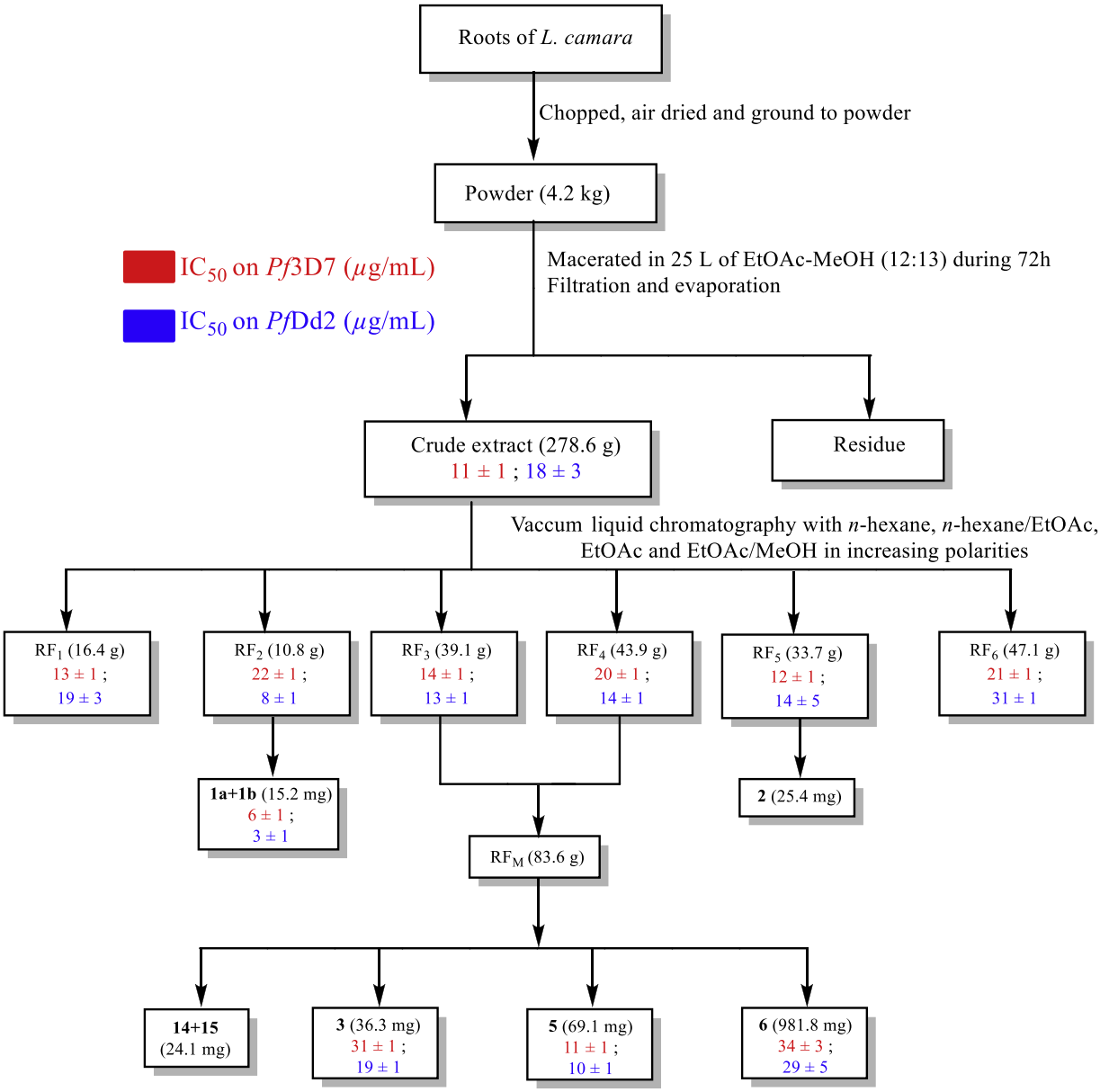

Fig. 5. Protocol of extraction and isolation of compounds from roots of L. *camara*.

μg/mL]) and strong (IC_{50} 12.10 μM [2.59 μg/mL]) activity against *Pf*3D7 and *Pf*Dd2, respectively (Table 3). Besides, we observed that compound (12) exhibited notable activity against the susceptible strains (3D7) of *P. falciparum*, achieving an IC_{50} value of 8.51 μM. However, when compared to established antimalarial standards, this compound was found to be significantly less potent, 430-fold less effective on the sensitive (3D7) strains. Moreover, when comparing the efficacy of isolated active chemicals against multidrug-resistant strains (Dd2), artemisinin and chloroquine were observed to be 121-fold and 10.80-fold more potent than the most active isolated compound. Despite its lower potency in comparison to existing therapies, the activity of the prioritised isolated compound against resistant strains is particularly noteworthy. This observation suggests that it may operate via a novel mechanism of action, presenting a potential platform for further optimization and development. Nonetheless, it is important to underscore the considerable efficacy gap that remains, highlighting an urgent need for accelerated research aimed at enhancing the activity of such compounds. Due to their interesting potency against multidrug-resistant strains, oleanonic acid (**5**), diodantunezone (**1a**), and isodiodantunezone (**1b**) could represent good candidates for further studies, such as structure-activity relationship, pharmacodynamics, and pharmacokinetics studies, before *in vivo* validation of antimalarial efficacy using a malaria murine model. We believe that the strong antiplasmodial potency of these compounds is attributable to the existence of the furan ring and the phenolic group, as these skeletons promote the generation of free radicals, leading to parasite death. To the best of our knowledge, this is the first report documenting the antiplasmodial activity and selectivity of L. *camara* extracts, fractions, and compounds.

4.3. Cytotoxicity results

The *in vitro* cytotoxicity assay revealed that some isolated compounds **1a** + **1b, 3, 4, 10a** + **10b, 13**, and **15** exhibited no toxicity, with half-maximal cytotoxic concentrations (CC_{50}) values greater than 100 μg/mL (Table 4). Compounds **2, 5**, and **6** demonstrated varying levels of inhibition, with CC_{50} values recorded between 16.71 to 31.98 μg/mL. These results suggest that L. *camara* is a potential source of non-toxic molecules, making it a promising candidate for further investigation

Table 2
Antiplasmodial activity and resistance index of fractions from leaf and root extracts of L. *camara* against *Plasmodium falciparum* strains.

Plants parts	Fraction codes	Antiplasmodial activity IC_{50} ± SD (μg/mL)		Resistance Index: IC_{50}*Pf*Dd2/IC_{50}*Pf*3D7
		***Pf*3D7**	***Pf*Dd2**	
Leaves	FFHLC	14.30 ± 1.54	22.69 ± 5.99	1.58
	FFALC	13.89 ± 0.98	25.41 ± 4.2284	1.82
	Ffnbu	84.49 ± 4.50	> 100	–
Roots	R_1LC	12.90 ± 0.97	18.86 ± 3.35	1.46
	R_2LC	21.90 ± 0.54	7.73 ± 1.10	0.35
	R_3LC	14.34 ± 1.32	13.22 ± 0.75	0.92
	R_4LC	19.91 ± 0.18	14.37 ± 0.36	0.72
	R_5LC	11.94 ± 0.19	13.80 ± 4.90	1.15
	R_6LC	21.71 ± 1.07	30.63 ± 0.98	1.10
Positive Control	Artemisinin (μM)	0.03 ± 0.00	0.05 ± 0.01	1.66
	Chloroquine (μM)	0.02 ± 0.00	0.56 ± 0.10	28

Table 3
Antiplasmodial activity and resistance index of some isolated compounds from L. *camara* against *Plasmodium falciparum* strains.

Plants parts	Compounds	Antiplasmodial activity IC_{50} ± SD (μM)		Resistance Index: IC_{50}*Pf*Dd2/IC_{50}*Pf*3D7
		***Pf*3D7**	***Pf*Dd2**	
Leaves	**3**	55.57 ± 1.82	34.49 ± 0.07	0.62
	5	24.60 ± 1.34	20.79 ± 2.62	0.84
	10a + **10b**	140.82 ± 4.36	71.40 ± 4.03	0.50
	13	79.54 ± 8.16	55.77 ± 0.16	0.70
	15	104.13 ± 11.68	55.24 ± 1.09	0.53
Roots	**1a** + **1b**	28.27 ± 3.41	12.10 ± 1.63	0.42
	5	24.60 ± 1.34	20.79 ± 2.62	0.84
	6	74.95 ± 7.39	64.67 ± 10.28	0.86
	12	8.51 ± 3.67	–	0.54
Positive Control	Artemisinin (μM)	0.03 ± 0.00	0.05 ± 0.01	1.66
	Chloroquine (μM)	0.02 ± 0.00	0.56 ± 0.10	28

in the search for novel, potent, and selective antimalarial chemotypes.

4.4. Haemolysis results

The haemolytic effect of the compounds was evaluated to assess their selectivity against erythrocytes (the parasite's host) and their specificity for intraerythrocytic *P. falciparum*. The results showed that antiplasmodial hit compounds exhibited very low haemolysis percentages, ranging from 1.59 to 37.16 % at a single concentration of 200 μg/mL, compared to the standard control Triton X-100 (100 % haemolysis) (Figs. 6 and 7). These results suggest that L. *camara* is a promising source of non-toxic molecules that could contribute to the development of

Table 4
In vitro cytotoxicity of some compounds isolated from L. *camara* against VERO cells Conc.

	Compounds	CC50 ± SD (μg/mL)	SI	
			***Pf*3D7**	***Pf*Dd2**
	1a + **1b**	> 100	> 16.52	> 38.61
	2	17.71 ± 1.66	–	–
	3	> 100	> 3.25	> 5.25
	4	> 100	–	–
	5	30.33 ± 1.64	2.71	3.21
	6	18.87 ± 2.16	0.55	0.63
	10a + **10b**	> 100	> 1.10	> 2.18
	13	> 100	> 2.06	> 2.93
	15	> 100	> 1.66	> 3.14
Positive Control	**PODO (μM)**	**0.016 ± 0.001**	**–**	**–**

novel and safe antimalarial drugs.

5. Computer-based forecasting of pharmacokinetic characteristics and drug-like attributes

The pharmacokinetics properties (ADMET) of the promising active compounds were assessed to support their further use as drug candidates. As a result, compounds **1a, 1b**, and **5**, which meet all the assessed bioavailability criteria, exhibit an intestinal absorption rate exceeding 92 %, as shown in Table 6 (100 % for compound **5**, 95.787 % for compound **1a**, and 95.921 % for compound **1b**). The non-saturable nature of the digestive tract membrane allows these lead compounds to pass through easily via passive transport (Zoete et al., 2011). Importantly, their skin permeability values indicate suitability for intradermal or transdermal delivery (−2.726 for compound **5**, −2.926 for compound **1a**, and −2.912 for compound **1b**). Besides, the lower the log Kp value, the reduced skin permeability of a molecule. The compounds analysed show favourable pharmacokinetics for oral or topical administration due to their high intestinal absorption rate (HIA > 90 %) and good skin permeability (log Kp > −2.5) (Daoui et al. 2022; Fouedjou et al. 2022). The prediction of water solubility in a crucial criterion in the *in vitro* drug optimization stage (Xiong et al., 2021; Dzeumo et al., 2022), and assessing this parameter indicates that all the investigated compounds exhibit water solubility values of −4.023, −2.763, and −2.651 for compounds **5, 1b**, and **1a**, respectively, which are more favourable than those of chloroquine (−4.249) and artemisinin (−3.678) use as reference.

The volume of distribution (VDss) for compounds exceeding 1.1 kg^{-1} indicates storage in body compartments or strong binding affinity. All tested compounds, except compound **5**, had VDss values below this threshold, while compounds **1a** and **1b** exhibited plasma distribution (log VDss < −0.15), with values of −0.053 and 0.092, respectively. In contrast, compound **5** had a higher VDss, suggesting tissue distribution. In addition, the unbound fractions of compounds **1a** and **1b** (0.364 and 0.357, respectively) exceeded 1/5, indicating that only this portion can interact with pharmacological target proteins, including enzymes, receptors, and channels. This fraction is also capable of diffusing between plasma and tissues, thereby underscoring its significant antiplasmodial activity.

The limited permeability of the blood-brain barrier (BBB) and the central nervous system (CNS) serves to safeguard these areas from harmful molecules. The log PS and log BB values for compounds **5, 1a**, and **1b** (−0.274, −0.083, and −0.08, respectively) are all below 0, indicating that only minimal quantities of these substances will penetrate these biological compartments. Moreover, low BBB permeability suggests sluggish transport into the brain, along with slow clearance from it for compounds that exhibit relatively high brain penetration (Szakàcs et al., 2008; Watanabe et al., 2018).

Cytochrome P450 (CYP450) interacts with various molecules that can activate or inhibit enzymes. In adults, the main CYP families for drug

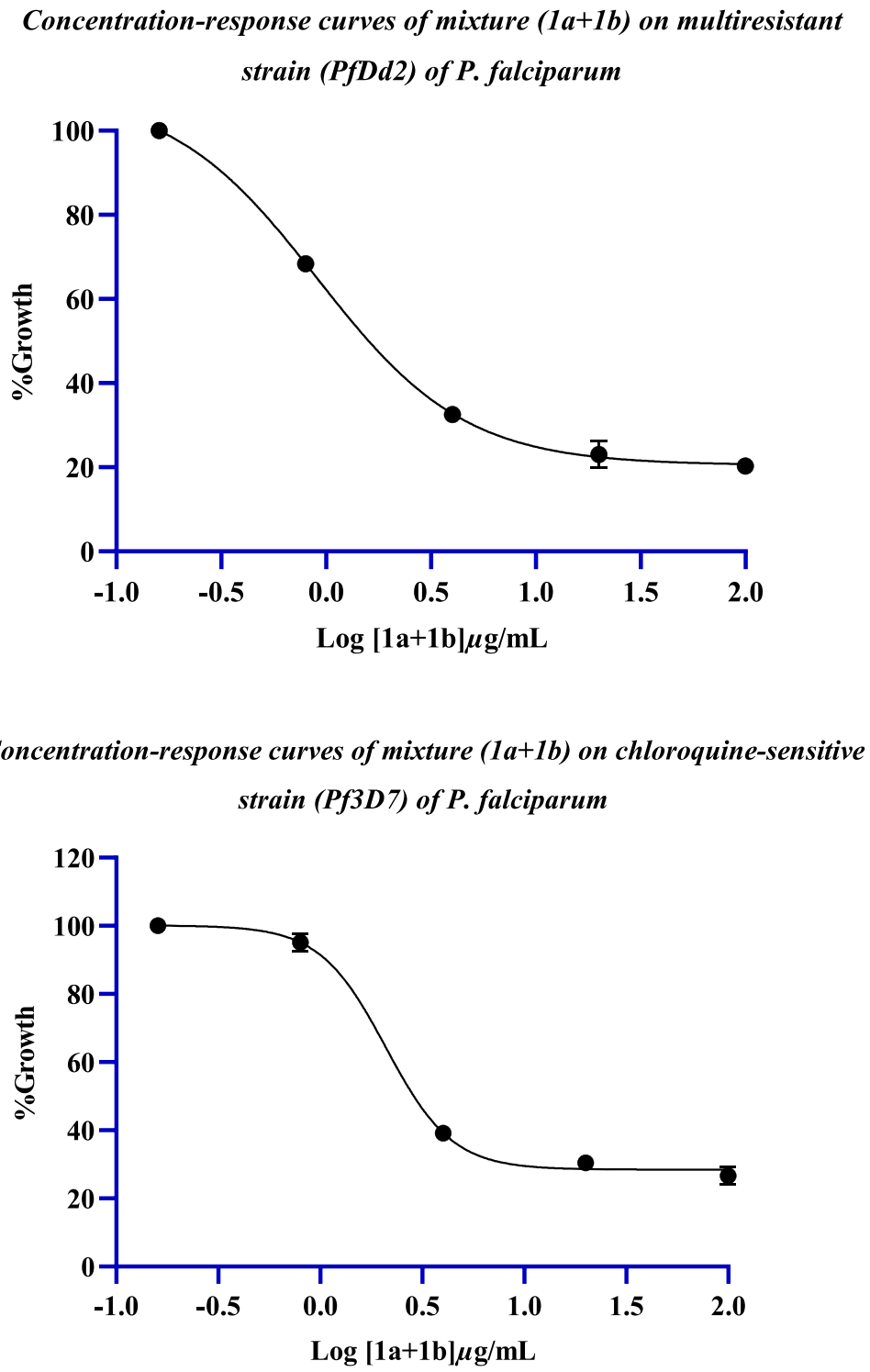

Fig. 6. Concentration-response curves of compound LCR2 (**2**) against multiresistant (*Pf*Dd2) and sensitive (*Pf*3D7) strains of *Plasmodium falciparum*. Data were normalized to percent control activity and median inhibitory concentrations (IC_{50s}) calculated using Prism 8.0 software (GraphPad) with data fitted by nonlinear regression to the variable slope sigmoidal dose-response formula $y = 100/[1 + 10(\log IC_{50} - x)\ H]$, where H is the Hill coefficient or slope factor.

metabolism are CYP 1, 2, and 3, with 70 % of liver cytochromes made up of seven key isoenzymes: CYP 1A2, 2A6, 2B6, 2C, 2D6, 2E1, and 3A (Fouedjou et al., 2022). Moreover, we assessed the interactions of cytochrome P450 (CYP) with candidate drug molecules in relation to five enzymes: 1A2, 2C9, 2C19, 2D6, and 3A4, which are crucial for drug metabolism (Fouedjou et al., 2022; Daoui et al., 2021) and the results as depicted in Table 6 show that none of the compounds are metabolized by CYP2D6, while only compound **5** was shown to be oxidized by CYP3A4. Additionally, except for compounds **1a** and **1b**, which inhibit CYP1A2, the remaining compounds do not inhibit the four cytochrome enzymes: 2C9, 2C19, 2D6, and 3A4. Isoform 3A4 plays a pivotal role in drug metabolism in the human body, indicating that the structures of compounds **5, 1a**, and **1b** are well-suited for metabolic processes within humans. In contrast, the total clearance (lol mL min^{-1} kg^{-1}) of compound **5** was < 0, indicating that its half-life is greater than those of the other compounds. Referring to the selectivity prediction, compounds **5, 1a**,

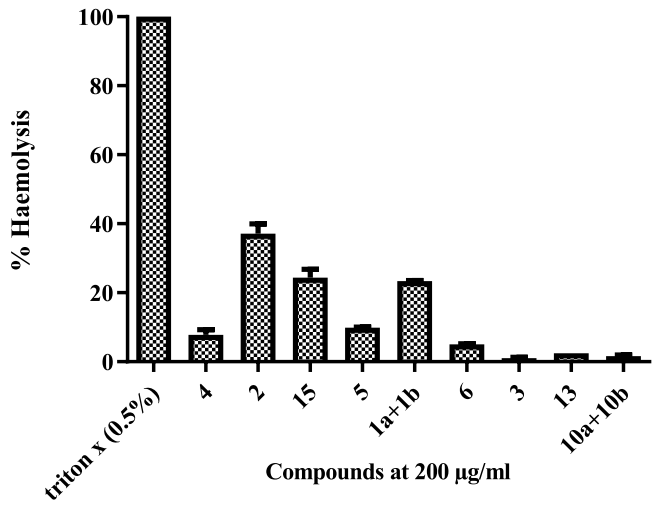

Fig. 7. Histogram representing the percentage of haemolysis (cytotoxicity on erythrocytes) of some isolated compounds.

and **1b**, with high LOAELs (2.169, 1.494, and 1.349, respectively), are less susceptible to chronic intoxication. Moreover, the AMES test and evaluations of hepatotoxicity showed that the structures of compounds **5, 1a**, and **1b** do not contribute to the hepatotoxicity or other undesirable side effects (Fig. 7). Consequently, these molecules can serve as promising initial candidates for effective antimalarial drug development.

6. Conclusion

The antiplasmodial evaluation of L. *camara* extract provides robust scientific validation for its traditional use in malaria treatment. Notably, the identified furanonaphthoquinones and triterpenoids could play a significant role in malaria drug discovery. Among the compounds assessed, the binary mixture of diodantunezone and isodiodantunezone demonstrated the highest antiplasmodial activity, particularly effective against chloroquine-resistant strains of *Plasmodium falciparum*. These findings pave the way for the development of enhanced traditional medicines (ETMs), contributing to improved health outcomes and living standards in affected communities. Further research should focus on the one hand, on the *in vitro* study of the decoction form of L. *camara* (the traditionally used form), and on the other hand, on the isolation and characterization of the antiplasmodial action of diodantunezone and

Table 6
Computer-based forecasting of the pharmacokinetic characteristics and drug-like attributes of the most promising antiplasmodial molecules.

Model Name	Predicted Value				Unit/classification
	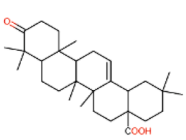	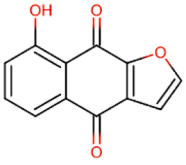	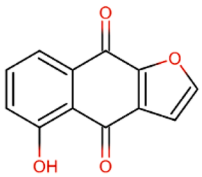	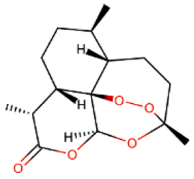	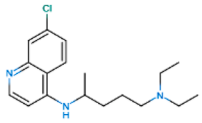	
	5	**1b**	**1a**	**Artemisinin**	**Chloroquine**	
Absorption						
Water solubility	−4.023	−2.763	−2.651	−3.678	−4.249	Numeric (log mol/L)
Caco2 permeability	1.303	0.969	1.07	1.295	1.624	Numeric (log Papp in 10–6 cm/s)
Intestinal absorption (human)	100	95.921	95.787	97.543	89.95	Numeric (% Absorbed)
Skin Permeability	−2.726	−2.912	−2.926	−3.158	−2.679	Numeric (log Kp)
P-glycoprotein substrate	No	Yes	Yes	No	Yes	Categorical (Yes/No)
P-glycoprotein I inhibitor	No	No	No	No	No	Categorical (Yes/No)
P-glycoprotein II inhibitor	Yes	No	No	No	No	Categorical (Yes/No)
Distribution						
VDss (human)	−0.968	0.092	−0.053	0.457	1.332	Numeric (log L/kg)
Fraction unbound (human)	0	0.357	0.364	0.4	0.191	Numeric (Fu)
BBB permeability	−0.274	−0.083	−0.08	0.235	0.349	Numeric (log BB)
CNS permeability	−0.992	−2.81	−2.809	−2.909	−2.191	Numeric (log PS)
Metabolism						
CYP2D6 substrate	No	No	No	No	Yes	Categorical (Yes/No)
CYP3A4 substrate	Yes	No	No	Yes	Yes	Categorical (Yes/No)
CYP1A2 inhibitior	No	Yes	Yes	Yes	No	Categorical (Yes/No)
CYP2C19 inhibitior	No	No	No	No	No	Categorical (Yes/No)
CYP2C9 inhibitior	No	No	No	No	No	Categorical (Yes/No)
CYP2D6 inhibitior	No	No	No	No	Yes	Categorical (Yes/No)
CYP3A4 inhibitior	No	No	No	No	No	Categorical (Yes/No)
Excretion						
Total Clearance	−0.133	0.005	0.041	0.98	1.092	Numeric (log mL/min/kg)
Renal OCT2 substrate	No	No	No	No	Yes	Categorical (Yes/No)
Toxicity						
AMES toxicity	No	Yes	Yes	Yes	Yes	Categorical (Yes/No)
Max. tolerated dose (human)	0.571	0.237	0.098	0.065	−0.167	Numeric (log mg/kg/day)
hERG I inhibitor	No	No	No	No	No	Categorical (Yes/No)
hERG II inhibitor	No	No	No	No	Yes	Categorical (Yes/No)
Oral Rat Acute Toxicity (LD50)	2.679	1.942	2.107	2.459	2.85	Numeric (mol/kg)
Oral Rat Chronic Toxicity (LOAEL)	2.169	1.349	1.494	1	1.026	Numeric (log mg/kg_bw/day)
Hepatotoxicity	No	No	No	No	Yes	Categorical (Yes/No)
Skin Sensitization	No	No	No	No	No	Categorical (Yes/No)
T.Pyriformis toxicity	0.286	1.037	0.942	0.322	1.558	Numeric (log ug/L)
Minnow toxicity	−1.794	0.878	0.992	1.406	0.747	Numeric (log mM)

isodiodantunezone individually. Additionally, investigating their pharmaco-modulations through hits-to-lead optimization can populate the drug discovery pipeline with innovative, naturally-derived antimalarial chemical pharmacophores.

Data availability

All data generated for this study are included in the article/supplementary material.

CRediT authorship contribution statement

Pierre Leonel K.Tafokeu Taguimjeu: Writing – original draft, Software, Resources, Methodology, Investigation, Data curation, Conceptualization. **Mariscal Brice Tchatat Tali:** Validation, Software, Methodology, Investigation, Formal analysis, Data curation, Conceptualization. **Kevine Johane Jumeta Dongmo:** Software, Methodology, Formal analysis, Data curation. **Yannick Stéphane Fotsing Fongang:** Writing – review & editing, Validation, Supervision, Methodology, Investigation, Conceptualization. **Marie-Laure Fauconnier:** Writing – review & editing, Validation, Supervision, Methodology, Conceptualization. **Bruno Ndjakou Lenta:** Writing – review & editing, Validation, Resources, Conceptualization. **Fabrice Fekam Boyom:** Writing – review & editing, Validation, Methodology. **Norbert Sewald:** Writing – review & editing, Validation, Resources, Conceptualization. **Silvère Augustin Ngouela:** Writing – review & editing, Validation, Supervision, Methodology.

Declaration of competing interest

The authors declare that they have no known competing financial interests or personal relationships that could have appeared to influence the work reported in this paper.

Acknowledgments

The authors thank the Yaoundé-Bielefeld Graduate School of Natural Products with Antiparasitic and Antibacterial activities (YaBiNaPa project N° 57561808) for materials support and the Laboratory of Chemistry of Natural Molecules, University of Liège, Gembloux Agro-Bio Tech (Belgium) for their scientific contribution. The contribution of Mr. Victor Nana, an experienced and retired botanist at the National Herbarium of Cameroon for plant collection and identification is also duly acknowledged.

Funding

This research did not receive any specific grant from funding agencies in the public, commercial, or not-for-profit sectors.

Supplementary materials

Supplementary material associated with this article can be found, in the online version, at doi:10.1016/j.sajb.2025.07.039.

References

Aman, D., 2019. Introductory chapter: plant extracts. https://doi.org/10.5772/intechopen.85493.

Ariey, F., Witkowski, B., Amaratunga, C., Beghain, J., Langlois, A., Khim, N., Kim, S., Duru, V., Bouchier, C., Ma, L., Lim, P., Leang, R., Duong, S., Sreng, S., Suon, S., Meng, C.C., Mey, B.D., Menard, S., Ranger, W., Genton, B., Fandeur, T., Miotto, O., Ringwald, P., Le Bras, J., Berry, A., Fairhurst, R., Benoit-Vical, F., Mercereau-Puijalon, O., Ménard, D., 2014. A molecular marker of artemisinin resistant *plasmodium falciparum* malaria. Nature 505, 50–55. https://doi.org/10.1038/nature12876.

Asua, V., Conrad, M.D., Aydemir, O., Duvalsaint, M., Legac, J., Duarte, E., Tumwebaze, P., Chin, D., Cooper, R., Yeka, A., Kamya, M., Dorsey, G., Nsobya, S., Bailey, J., Rosenthal, P.J., 2021. Changing prevalence of potential mediators of aminoquinoline, antifolate, and artemisinin resistance across Uganda 223. J. Infect. Dis. 223 (6), 985–994. https://doi.org/10.1093/infdis/jiaa687.

Atanasov, A., Waltenberger, B., Pferschy-Wenzig, E., Linder, T., Wawrosch, C., Uhrin, P., Temmi, V., Wang, L., Schwaiger, S., Heiss, E., Rollinger, J., Schuster, D., Breuss, J., Bochkov, V., Mihovilovic, M., Kopp, B., Bauer, D.V.M., Stuppner, H., 2015. Discovery and resupply of pharmacologically active plant derived natural products: a review. Biotechnol. Adv. 33, 1582–1614. https://doi.org/10.1016/J.biotechadv.2015.08.001.

Baba, G., Adewumi, A.A.J., Aina, V.O., 2011. Phytochemical characterization and *in-vivo* anti-malaria activity of *Lantana camara* leaf extract. British J. Pharmacol. Toxicol. 2 (6), 277–282.

Barre, T., Bowden, F., Coll, C., De Jesus, J., De la Fuente, E., Janairo, G., Ragassa, C., 1997. A bioactive triterpene from *Lantana camara*. Phytochemistry 45, 321–324. https://doi.org/10.1016/S0031-9422(96)00805-9.

Boakye, Y.D., Agana, T.A., Oteng-Amankwah, E.A., Boamah, V.E., Agyare, C., 2023. Evidence-based review of medicinal plants for the management of onchocerciasis. Nat. Product. Vector-Borne Dis. Manag. 27–49. https://doi.org/10.1016/B978-0-323-91942-5.00004-5.

Bowling, T., Mercer, L., Don, R., Jacobs, R., Nare, B., 2012. Application of a resazurin-based high-throughput screening assay for the identification and progression of new treatments for human African trypanosomiasis. Int. J. Parasitol. 2, 262–270. https://doi.org/10.1016/j.ijpddr.2012.02.002.

Cameron, M., Callender, E., Kramer, J., 1972. NMR studies of selected cholesteric compounds. Molecul. Cryst. Liquid Cryst. 3, 867–877. https://doi.org/10.1080/15421407208083581.

Cullen, J.M., Stalker, M.J., 2016. Liver and biliary system. Jubb.,Kennedy Palmer's Pathol. Dom. Anim. 2, 258–352. https://doi.org/10.1016/B978-0-7020-5318-4.00008-5 e1.

Cock, I.E., Van Vuuren, S.F., 2020. The traditional use of southern African medicinal plants in the treatment of viral respiratory diseases: a review of the ethnobotany and scientific evaluations. J. Ethnopharmacol. 262, 113194. https://doi.org/10.1016/j.jep.2020.113194.

Daoui, O., Elkhattabi, S., Chtita, S., Elkhalabi, R., Zgou, H., Benjelloun, A.T., 2021. QSAR, molecular docking and ADMET properties *in silico* studies of novel 4,5,6,7-tetrahydrobenzo [D]-thiazol-2-yl derivatives derived from dimedone as potent anti-tumor agents through inhibition of C-Met receptor tyrosine kinase. Heliyon 7, e07463. https://doi.org/10.1016/j.heliyon.2021.e07463.

Daoui, O., Mazoir, N., Bakhouch, M., Salah, M., Benharref, A., Gonzalez-Coloma, A., Elkhattabi, S., Yazidi, M.E., Chita, S., 2022. 3D-QSAR, ADME-tox, and molecular docking of semisynthetic triterpene derivatives as antibacterial and insecticide agents. Struct. Chem. 33, 1063–1084. https://doi.org/10.1007/s11224-022-01912-4.

Delgado-Altamirano, R., Garcia-Aguilera, E., Delgado-Dominguez, J., Becker, I., Rodriguez, D.S.M., Rojas-Molinas, A., Esturau-Escofet, N., 2021. ^{1}H NMR profiling and chemometric analysis as an approach to predict the leishmanicidal activity of dichloromethane extracts from *Lantana camara* (L.). J. Pharm. Biomed. Anal. 199, 114060–114068. https://doi.org/10.1016/j.jpba.2021.114060.

Dibong, S.D., Mpondo, M.E., Ngoye, A., Kwin, M.F., Betti, J.L., 2011. Ethnobotanique et phytomédecine des plantes médicinales de Douala, Cameroun [Ethnobotany and phytomedicine of medicinal plants sold in Douala markets]. J. Appl. Biosci. 37, 2496–2507.

Dominguez, A., Franco, R., Cano, G., Garcia, F., Consue, L., Dominguez, S., Xorge, A., Leonardo, M., 1983. Mexican medicinal plants. Part 47. Isolation of a new furano-1,4-naphthaquinones, diodantunezone from *Lantana achyranthifolia*. Planta Med. 49, 63. https://doi.org/10.1055/s-2007-969816.

Dongmo, J., Tali, T., Fongang, F., Taguimjeu, T., Kagho, K., Bitchagno, T., Lenta, N., Boyom, F., Sewald, N., Ngouela, A., 2023. *In vitro* antiplasmodial activity and toxicological profile of extracts, fractions and chemical constituents of leaves and stem bark from *Dacryodes edulis* (Burseraceae). BMC Complement. Med. Therap. 23, 211. https://doi.org/10.1186/s12906-023-03957-2.

Dzeumo, L.C., Happi, G.M., Ahmed, S.A., Tsopgni, W.D.T., Akuma, M.N., Salau, S., Happi, E.N., Wansi, J.D., 2022. Chemical constituents of the bark of *zanthoxylum gilletii* (Rutaceae) and their *in vitro* antiplasmodial and molecular docking studies. J. Chem. ID 1111817, 1–10. https://doi.org/10.1155/2022/1111817.

FajriahS, M., Darmawan, A., 2016. Apigenin, an anticancer isolated from *Macaranga gigantifolia* leaves. J. Tropic. Life Sci. 6 (1), 7–9.

Fongang, S., Bankeu, J., Batiha, G., Ali, I., Lenta, B., 2021. Extraction of bioactive compounds from medicinal plants and herbs. Medicinal *Plants*. IntechOpen Pharmacognosy. https://doi.org/10.5772/intechopen.98602.

Fouedjou, R.T., Daoui, O., Nour, H., Ayoub, M., Fogang, H.P.D., Siddique, F., Elkhattabi, S., Bakhouch, M., Belaidi, S., Chtita, S., 2022. *In silico* approach for designing novel SARS-CoV-2 inhibitors from medicinal plants. Phys. Chem. Res. 11 (3), 589–604. https://doi.org/10.22036/pcr.2022.349693.2138.

Ghallab, D.S., Mohyeldin, M.M., Shawky, E., Metwally, A.M., Ibrahim, R.S., 2021. Chemical profiling of Egyptian propolis and determination of its xanthine oxidase inhibitory properties using UPLC-MS/MS and chemometrics. LWT- Food Sci. Technol. 136, 110298. https://doi.org/10.1016/j.lwt.2020.110298.

Herbert, J.M., Maffrand, J.P., Taoubi, K., Augereau, J.M., Fouraste, I., Gleye, J., 1991. Verbascoside isolated from *Lantana camara*, an inhibitor of protein kinase C. J. Nat. Prod. 54 (6), 1595–1600. https://doi.org/10.1021/np50078a016.

Kambele, K., Mukubwa, K., Mwabonkolo, M., Musuyu, M., Nkanga, I., Memvanga, B., 2022. *In vivo* antimalarial activity of self-nanoemulsifying drug delivery systems containing ethanolic extract of *Morinda lucida* in combination with other Congolese plants extracts. Brazil. J. Pharmaceutic. Sci. 58, e20074. https://doi.org/10.1590/s2175-97902022e20074.

Kaushik, N., Sharma, J., Sahal, D., 2012. Anti-plasmodial action of de novo designed, cationic, lysine-branched, amphipathic, helical peptides. Malar. J. 11, 256. https://doi.org/10.1186/1475-2875-11-256.

Lambros, C., Vanderberg, J., 1979. Synchronization of *plasmodium falciparum* erythrocytic stages in culture. J. Parasitol. 65, 418. https://doi.org/10.2307/3280287.

Mahato, S., Kundu, A., 1994. ^{13}C NMR spectra of pentacyclic triterpenoids – A compilation and some salient features. Phytochemistry 37, 1517–1575. https://doi.org/10.1016/S0031-9422(00)89569-2.

Mahwasane, S.T., Middleton, L., Boaduo, N., 2013. An ethnobotanical survey of indigenous knowledge on medicinal plants used by the traditional healers of the Lwamondo area, Limpopo province, South Africa. South African J. Botany. 88, 69–75. https://doi.org/10.1016/j.sajb.2013.05.004.

Mangoyi, R., Midiwo, .J, Mukanganyama, S., 2015. Isolation and characterization of an antifungal compound 5-hydroxy-7,4'-dimethoxyflavone from *Combretum zeyheri*. BMC Complement. Altern. Med. 15, 405. https://doi.org/10.1186/s12906-015-0934-7.

Mayori, A., 2017. Traditional usage, phytochemistry and pharmacology of *Croton sylvaticus* Hochst. Ex. In: Krauss, C. (Ed.), Traditional usage, phytochemistry and pharmacology of *Croton sylvaticus* Hochst. Ex. Asian. Pac. J. Trop. Med. 10 (5), 423–429. https://doi.org/10.1016/j.apjtm.2017.05.002.

Muganza, D.M., Fruth, B., Nzunzu, J.L., Tuenter, E., Foubert, K., Cos, P., Maes, L., Kanyanga, R.C., Exarchou, V., Apers, S., Pieters, L., 2016. *In vitro*antiprotozoal activity and cytotoxicity of extracts and isolated constituents from *Greenwayodendron suaveolens*. J. Ethnopharmacol. 193, 510–516. https://doi.org/10.1016/j.jep.2016.09.051.

Nea, F., Bitchi, M.B., Genva, M., Ledoux, A., Tchinda, A.T., Damblon, C., Frederich, M., Tonzibo, Z.F., Fauconnier, M.-L., 2021. Phytochemical investigation and biological activities of *Lantana rhodesiensis*. Molecules 26 (4), 846. https://doi.org/10.3390/molecules16053663.

Njoroge, G.N., Bussmann, R.W., 2006. Diversity and utilization on antimalarial ethnophytotherapeutic remedies among the Kikuyus (Central Kenya). J. Ethnobiol. Ethnomed. 2 (8). https://doi.org/10.1186/1746-4269-2-8.

Nkengasong, N., Tessema, S., 2020. Africa needs a new public health order to tackle infectious disease threats. Cell Press. 183 (2), 296–300. https://doi.org/10.1016/j.cell.2020.09.041.

Ntiga, L., 2008. Cameroun: *lantana Camara* - une thérapie contre les filaires. Mutations. https://fr.allafrica.com/stories/200809030947.html. consulted online on October 11th, 2024.

Pires, D., Blundell, T., Ascher, D., 2015. pkCSM: predicting small-molecule pharmacokinetic and toxicity properties using graph-based signatures. J. Med. Chem. 58, 4066–4072. https://doi.org/10.1021/acs.jmedchem.5b00104.

Qureshi, H., Anwar, T., Ali, Q., Haider, M.Z., Habib, N., Fatima, S., Waseem, M., Bibi, Y., Arshad, M., Adkins, S.W., 2019. Isolation of natural herbicidal compound from *Lantana camara*. Int. J. Environ. Anal. Chem. 101 (5), 631–638. https://doi.org/10.1080/03067319.2019.1670822.

Ramaraj, D.J., Rathinasamy, G., Sivasamy, V.V., 2018. Isoaltion of eupatorin form *Albizia odorotissima* and its application for *L*-tryptophan sensing. Res. Chem. Intermed. 44, 6917–6931.

Rosenthal, P., 2021. Are artemisinin-based combination therapies for malaria beginning to fail in Africa. Am. J. Tropic. Med. Hygiene 105 (4), 857–858. https://doi.org/10.4269/ajtmh.21-0797.

Sato, S., 2021. *Plasmodium* – a brief introduction to the parasites causing human malaria and their basic biology. J. Physiol. Anthropol. 40 (1), 1–13. https://doi.org/10.1186/s40101-020-00251-9.

Shipa, S.J., Khandokar, L., Bari, M.S., Qais, N., Rashid, M.A., Haque, M.A., Mohamed, I. N., 2022. An insight into the anti-ulcerogenic potentials of medicinal herbs and their bioactive metabolites. J Ethnopharmacol 293, 115245. https://doi.org/10.1016/j.jep.2022.115245.

Sinha, S., Batovska, D.I., Medhi, B., Radotra, B.D., Bhalla, A., Markova, N., Sehgal, R., 2019. *In vitro* anti-malarial efficacy of chalcones: cytotoxicity profile, mechanism of action and their effect on erythrocytes. Malar J 18 (1), 421. https://doi.org/10.1186/s12936-019-3060-z.

Smilkstein, M., Sriwilaijaroen, N., Kelly, X., Wilairat, P., Riscoe, M., 2004. Simple and inexpensive fluorescence-based technique for high-throughput antimalarial drug screening. Antimicrob. Agents Chemother. 48, 1803–1806. https://doi.org/10.1128/AAC.48.5.1803-1806.2004.

Smit, F., van Biljon, R., Birkholtz, L., N'Da, D., 2015. Synthesis and *in vitro* biological evaluation of dihydroartemisinyl-chalcone esters. Eur. J. Med. Chem. 90, 33–44. https://doi.org/10.1016/j.ejmech.2014.11.016.

Sousa, E., Braz-Filho, R., Coutinho, M., Menezes, R., Rodrigues, G., Costa, M., 2018. New 13^2-epi- phaeophorbide-a ethyl ester from *Lantana camara*. Chem. Nat. Compound. 54 (6), 1114–1116. https://doi.org/10.1007/s10600-018-2567-9.

Stensen, W.G., Jensen, E., 1995. Structural determination of 1,4-naphthoquinones by mass spectrometry/mass spectrometry. J. Mass Spectrom. 30, 1126–1132. https://doi.org/10.1002/jms.1190300809.

Suryati, S., Malasari, Y., Efdi, M., Mardiah, E., 2019. A cytotoxic compound from n-hexane fraction of *Lantana camara* Linn Leaves. Molekul 14 (1), 31–36. https://doi.org/10.20884/1.jm.2019.14.1.477.

Szakàcs, G., Vàradi, A., Özvegy-Laczka, C., Sarkadi, B., 2008. The role of ABC transporters in drug absorption, distribution, metabolism, excretion and toxicity (ADME-Tox). Drug Discov. Today 13, 379–393. https://doi.org/10.1016/j.drudis.2007.12.010.

Tabudi, J.R.S., 2008. Herbal medicines used in the treatment of malaria in Budiope county, Uganda. J. Ethnopharm. 116, 33–42. https://doi.org/10.1016/j.jep.2007.10.036.

Taguimjeu, P.L.K.T., Fongang, Y.S.F., Genva, M., Shinyuy, L.M., Held, J., Frederich, M., Ngouela, S.A., Fauconnier, M.-L., 2025. Antiplasmodial activity of a new chemotype of *Croton sylvaticus* Hochst. Ex C. Krauss essential oil. Int. J. Molecul. Sci. 26, 858. https://doi.org/10.3390/ijms26020858.

Tajbakhsh, E., Kwenti, T.E., Kheyri, P., Nezaratizade, S., Lindsay, D.S., Khamesipour, F., 2021. Antiplasmodial, antimalarial activities and toxicity of African medicinal plants: a systematic review of literature. Malar. J. 20, 349. https://doi.org/10.1186/s12936-021-03866-0.

Tali, T., Dize, D., Wouamba, N., Fokou, V., Keumoe, R., Ngansop, C., Njionhou, M., Mbouna, C., Tchokouaha, L., Maharaj, V., Khorommbi, K., Naidoo-Maharaj, D., Tchouankeu, J., Fekam, F., 2022. *In vitro* antiplasmodial activity-directed investigation and UPLC-MS fingerprint of promising extracts and fractions from *Terminalia ivorensis* A. Chev and *Terminalia brownii* Fresen. J. Ethnopharmcol. 296. https://doi.org/10.1016/j.jep.2022.115512.

Tamdem, M., Ntonga, A., Tsila, G., Tonga, C., Nkouandou, M., Djeukam, A., Ngaha, R., Ngo Hondt, E., Mbongue, R., Soh, T., Kamga, K., Foko, K., Dogmo, J., Menut, C., 2020. Biological activities of the essential oils of *Cupressus macrocarpa, Lantana camara* and *Psidium littorale* against *Plasmodium falciparum* welch, 1987 and *Anopheles gambiae* giles, 1902. J. Entomol. Zool. Stud. 8 (6), 854–862. https://doi.org/10.22271/j.ento.2020.v8.i6l.7949.

Tsague, M.A.I.M., 2019. Etude Floristique Et Ethnobotanique Des Plantes Antipaludéennes Du Département de La Vina (Adamaoua – Cameroun). Mémoire de Master, Université de Ngaoundéré, Ngaoundéré, Cameroun.

Venkatesalu, V., Gopalan, N., Pillai, R., Singh, V., Chandrasekaran, M., Senthilkumar, A., Chandramouli, N., 2012. *In vitro* anti-plasmodial activity of some traditionally used medicinal plants against *plasmodium falciparum*. Parasitol. Res. 111, 497–501. https://doi.org/10.1007/s00436-012-2834-9.

Watanabe, R., Esaki, T., Kawashima, H., Natsume-Kitatani, Y., Nagao, C., Ohashi, R., Mizuguchi, K., 2018. Predicting fraction unbound in Human plasma from chemical structure: improved accuracy in the low value range. Mol. Pharm. 15, 5302–5311. https://doi.org/10.1021/acs.molpharmaceut.8b00785.

Wen, X., Sun, H., Liu, J., Cheng, K., Zhang, P., Zhang, L., Hao, J., Zhang, L., Ni, P., Zographos, S.E., Leonidas, D.D., Alexacou, K.-M., Gimisis, T., Hayes, J.M., Oikonomakos, N.G., 2008. Naturally occurring pentacyclic triterpenes as inhibitory of glycogen phosphorylase: synthesis, structure-activity relationships, and X-ray crystallographic studies. J. Med. Chem. 51 (12), 3540–3554.

WHO, 2024. World Malaria Report 2024. Available online: https://www.who.int/teams/global-malaria-programme/reports/world-malaria-report-2024. (accessed on 14 January 2025).

WHO, 2023. World malaria report 2023. Geneva: World Health Organization; 2023. Licence: CC BY-NC-SA 3.0 IGO.

WHO, 2021a. World Health Organization, 2021a. World Malaria Report 2021, World Malaria Report. World Health Organization, Geneve.

WHO, 2021b. World Health Organization, 2021b. https://www.who.int/news/item/06-10-2021 who recommends-groundbreaking-malaria-vaccine-for-children-at-risk? Accessed on 22 March 2022.

WHO, 2020. World Health Organization, 2020. The E-2020 Eliminating 2019 progress report.

Xiong, G., Wu, Z., Yi, J., Li, F., Zhijiang, Y., Changyu, H., Mingzhu, Y., Xiangxiang, Z., Chengkun, W., Aiping, L., Xiang, C., Tingjun, H., Dongsheng, C., 2021. ADMET lab 2.0: an integrated online platform for accurate and comprehensive predictions of ADMET properties. Nucleic Acids Res. 49 (1), W5–W14. https://doi.org/10.1093/nar/gkab255.

Ye, M., Han, J., Chen, H., Zheng, J., 2007. Analysis of phenolic compounds in rhubarbs using liquid chromatography coupled with electrospray ionization mass spectrometry. J. Am. Soc. Mass Spectrom. 18, 82–91. https://doi.org/10.1016/j.jasms.2006.08.009.

Zhan, C., Xiong, A., Shen, D., Yang, L., Wang, Z., 2016. Characterization pf the principal constituents of Danning Tablets, a Chinese formula consisting of seven herbs, by an UPLC-DAD-MS/MS approach. Molecules 21, 631. https://doi.org/10.3390/molecules21050631.

Zoete, V., Cuendet, A., Grosdidier, A., Michielin, O., 2011. SwissParam: a fast force field generation tool for small organic molecules. J. Comput. Chem. 32 (11), 2359–2368. https://doi.org/10.1002/jcc.21816.